Investigation and detection of crack formations during micro electromechanical systems (MEMS) resonator manufacturing and use

Alaa Mahmoud Hassan Abdalla

School of Electrical Engineering

Thesis submitted for examination for the degree of Master of Science in Technology.

Espoo 31.7.2023

Supervisor

Prof. Ivan Vujaklija

Advisor

Anttoni Huhtala

Aalto University
School of Electrical
Engineering

Aalto University
School of Electrical
Engineering

Aalto University, P.O. BOX 11000, 00076 AALTO
www.aalto.fi
Abstract of the master's thesis

Author Alaa Mahmoud Hassan Abdalla

Title Investigation and detection of crack formations during micro electromechanical systems (MEMS) resonator manufacturing and use

Degree programme Smart systems integrated solutions

Major Smart systems integrated solution **Code of major** ELEC29

Supervisor Prof. Ivan Vujaklija

Advisor Anttoni Huhtala

Date 31.7.2023 **Number of pages** 60 **Language** English

Abstract

Time reference devices have been widely used in the industry for the past decades due to their important role in different devices applications such as portable and wearable device. With the rapid technology improvements in the semiconductor industry, micro-electromechanical systems (MEMS) resonators were presented as a time reference devices which offer a reduced cost and small size that facilitate the integration with the other electronics.

Because of the microfabrication processes and operational modes for MEMS-resonators, defects are expected to be formed in different stages of the manufacturing and use. Those defects would be costly if have not been detected in early stages, hence, industry dedicates time and resources for better detection of defects. With the mass production of MEMS-resonator, manual inspection of defects is becoming an impractical solution, that led to develop automation systems for defects' detection. This work studies the defects that may occur in MEMS-resonator in different stages and a studies defects detection methods. The study aims to investigate the microfabrication induced defects, the defects formation during the device operation and to develop an automatic defects inspection tool. To fulfil the study objectives, different MEMS-resonator devices were designed in order to study the effect of different parameters such as the geometry and dimensions on the robustness of the device. Standard microfabrication processes were implemented to observe the risk of defects formation during manufacturing. For the operation stage, FEM simulations were executed, and different mode shapes were selected to study the likelihood of mode shapes to produce defects for the device fragile parts. The last stage for defects inspection included implementation of automatic optical inspection (AOI) tool with a hardware setup for image collection and a software part for image processing and defection/robustness decision making, the result of the AOI was validated by the percentage of the detected defects and the occurrence of false-positives.

The MEMS-resonators designs considered 2 frequencies of 24MHz and 32MHz, 3 different anchors and 7 different beam widths with average resulting quality factor(Q) of 11.68×10^3. Common defects of AlN particles residuals were observed with SEM as a microfabrication caused defects. 8.4% of the devices were defected electrically by resonating in specific spurious modes, 19.89% of the resonator were defected after performing the tape-peeling test. AOI tool was successful to reach 85.5% detection rate with 7.1% false-positive occurrences.

Keywords MEMS, Resonator, Semiconductors, Piezoelectric, AOI, Spurious mode, SEM, FEM, Tape-peeling, Microfabrication, Microcracks

Preface

I want to thank Professor Ivan Vujaklija and my advisor Anttoni Huhtala for their effort, support and guidance to complete this work.
The support and help i found from KTO team made a remarkable push for my knowledge, understanding and my practical experience, that's why i want to give a special thanks for all teams working in KTO.
I extend my gratitude to my family and friends for the moral support that has been blessing me for the entire journey of my master studies.

Otaniemi, 31.7.2018

Alaa M. H. Abdalla

Contents

Abstract 3

Preface 5

Contents 6

Abbreviations 8

1 Introduction 9

2 Background 11
2.1 Concept of physical resonance . . . 11
2.1.1 Electrical Resonance . . . 12
2.1.2 Mechanical Resonance . . . 12
2.2 MEMS resonator importance and applications . . . 13
2.2.1 Timing and Frequency Reference . . . 13
2.2.2 Sensing . . . 14
2.2.3 Actuation . . . 14
2.2.4 Communication . . . 14
2.3 MEMS resonator materials and fabrications . . . 15
2.4 Resonance modes . . . 16
2.4.1 Bulk mode . . . 17
2.4.2 Flexural mode . . . 17
2.4.3 Coupled resonant mode . . . 17
2.5 Role of microfabrication on MEMS resonator quality . . . 19
2.6 MEMS devices defects formation . . . 20
2.6.1 Testing induced defects . . . 20
2.6.2 Operational defects . . . 20
2.7 MEMS devices defects detection . . . 21
2.7.1 Automated optical inspection (AOI) . . . 21
2.7.2 Electrical testing . . . 22

3 Research material and methods 24
3.1 MEMS resonator design . . . 24
3.1.1 MEMS resonator dimensions and anchor design . . . 24
3.1.2 Quality factor optimization . . . 24
3.1.3 Spurious mode analysis . . . 32
3.2 Defects inducing . . . 34
3.2.1 Electrical inducing . . . 34
3.2.2 Tape peeling test . . . 35
3.3 Defects inspection . . . 35
3.3.1 Optical inspection . . . 35

4 Results **37**
4.1 MEMS resonator design 37
4.1.1 24-MHz resonators 37
4.1.2 32-MHz resonators 37
4.2 Microfabrication processes 43
4.3 Electrical defects inducing 45
4.4 Tape peeling test 46
4.5 Automatic optical inspection 46

5 Discussion **49**
5.1 MEMS resonator design 49
5.2 Microfabrication defects 50
5.3 Defects inducing and detection 50

6 Conclusion **52**

References **54**

Abbreviations

MEMS	micro-elctromechanical systems
AOI	automated optical inspection
AC	alternating current
DC	direct current
LE	length extensional
FEM	finite element method
SEM	scanning electron microscope
RF	Radio frequency
CMOS	Complementary metal–oxide–semiconductor
SOI	Silicon-on-insulator
KTO	KYOCERA-tikitin oy

1 Introduction

Micro-Electro-Mechanical Systems (MEMS) resonators are miniature devices that combine mechanical and electrical properties on a microscale. These resonators play a crucial role in various industries and applications due to their unique characteristics and capabilities. These resonators consist of thin-film structures patterned and released on a substrate, resonance feature is gained from the piezoelectric material deposited on the silicon layer as shown in figure 1.

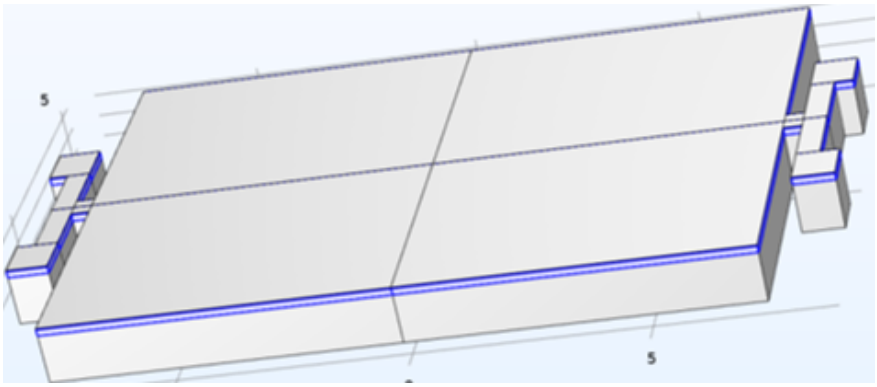

Figure 1: MEMS resonator structure highlighting the piezoelectric layer deposited between silicon layer and a conductive material layer on top

The importance of MEMS resonators stems from their ability to generate precise and stable oscillations at specific frequencies. These resonators serve as essential timing references [1], frequency filters, and clock sources in various electronic devices and systems. The accurate timing provided by MEMS resonators is crucial in telecommunications networks, data centers, and high-speed communication systems, enabling synchronization and coordination of multiple components.
One of the significant advantages of MEMS resonators is their miniaturization potential. Their compact size allows for integration with other electronic components on a single chip, reducing the overall footprint and power consumption of electronic devices [2]. This miniaturization has revolutionized industries like consumer electronics, medical devices, and automotive systems, where space constraints and portability are critical considerations.
MEMS resonators find applications across diverse industries, reflecting their versatility and adaptability. In wireless communication systems, they act as frequency-selective filters, providing improved signal quality and efficient communication. MEMS resonators are also utilized as accelerometers, gyroscopes, pressure sensors, and temperature sensors [3] in automotive, biological [4], and industrial monitoring systems [5]. Moreover, MEMS resonators serve as the primary clock source in electronic devices, replacing traditional quartz crystal oscillators [6]. This transition to MEMS-based oscillators offers several advantages, including lower power consumption [7], reduced cost, and seamless integration with other components. In consumer electronics like smartphones, tablets, and wearable devices [8], MEMS resonators ensure precise

timing for audio/video synchronization, data processing, and power management. Despite their significance, MEMS resonators are susceptible to various defects that can impair their performance and reliability. Common defects include structural issues such as cracks, deformations, or material inhomogeneities, material defects like impurities or contamination, and electrical connection problems [9]. These defects may arise during the manufacturing process or due to external factors like mechanical stress or environmental conditions.

The detection and characterization of defects in MEMS resonators are critical for ensuring their functional integrity. Manual defect detection can be labor-intensive and time-consuming and may not always identify subtle or hidden defects effectively. To overcome these limitations, automated defect detection techniques have emerged as powerful tools for quality control and reliability assessment.

Optical inspection techniques involve visual examination using microscopes or cameras to identify visible defects on the MEMS resonator's surface. Advanced imaging techniques, such as scanning electron microscopy (SEM) [10] and atomic force microscopy (AFM) [11], provide detailed characterization of defects at nanoscale resolution, allowing for precise defect analysis.

Non-destructive testing methods like acoustic microscopy and laser scanning enable defect detection without damaging the MEMS resonator. These techniques use acoustic or laser waves to probe the resonator's structure and identify internal defects or cracks.

With the mass production of MEMS resonator, continuous research aims to improve fabrication techniques, defect detection methods, and overall reliability of MEMS resonators to ensure their consistent performance and longevity in diverse applications [12]. Manual defect detection is an impractical solution and it can be time-consuming and may lack to precision, hence, automated defect detection techniques, such as optical inspection [13], advanced imaging, non-destructive testing, microstructural analysis, and electrical testing, offer faster and more accurate defect identification.

In this work, a study about defects formation on MEMS resonator will be discussed in an industrial framework in collaboration with Kyocera-tikitin oy (KTO) company, the study discusses the probability of defects formation throughout the different stages starting from design, microfabrication and then the operational mode of the devices, the work also studies the robustness of the devices based on the quality factor, geometry and dimensions by performing the tape peeling test. For the inspection part of the study, automated optical inspection tool was developed.

2 Background

The term (MEMS) or (micro-electro-mechanical systems), refers to a technology that can be defined as miniature mechanical and electro-mechanical components, which are created utilizing microfabrication processes. On the lower end of the size spectrum, the crucial physical dimensions of MEMS devices can range from much below one micron to several millimeters. Similar to how different MEMS device types can range from relatively straightforward structures with fixed parts to extremely complicated electromechanical systems with numerous moving parts managed by integrated microelectronics. MEMS devices are already employed in a wide range of sensing and actuation applications such as temperature, pressure, vibration sensing. The industry have achieved a few mm^3 size gyroscopes [14] and accelerometers [15] in the recent years.
Defects on MEMS devices have direct affect on their main physical properties and behaviour which can disturb their performance, for MEMS resonator, defects can result in a frequency shift, where the resonator operates at a different frequency than the intended value, moreover, defects can have several effects on the damping characteristics of the MEMS resonator [16]. Hence, it is essential to minimize defects during the fabrication process of MEMS resonators to ensure their desired performance and reliability [17]. Defects can be mitigated through careful design, precise fabrication techniques, quality control measures, and post-fabrication testing and inspection. To the aim of reducing the number of defected MEMS devices, different inspection techniques are held during and after the manufacturing for the MEMS devices, automation has been widely adopted by the industry specially after the mass production targeting time saving and standardized ways of inspection. These inspection ways differ from structural checks to performance and reliability tests.

2.1 Concept of physical resonance

The resonance physical concept refers to the phenomenon that occurs when an object is subjected to an external force that matches its natural frequency, causing it to vibrate with a large amplitude [18]. When an object is forced to vibrate at a frequency that matches its natural frequency, it will vibrate with a larger amplitude than if it were forced to vibrate at a different frequency. This phenomenon is known as resonance. The natural frequency of an object depends on its physical properties such as mass, stiffness, and geometry.
Resonance occurs in many physical systems, including mechanical systems, electrical circuits, acoustic and optical systems. It is a fundamental concept in fields such as acoustics, mechanics, and electromagnetic. Resonance has numerous practical applications, such as in musical instruments, electronics, and medical imaging.
The understanding of resonance phenomena is crucial for the efficient functioning of various devices and systems. Mathematical approaches such as the Fourier transform, the complex scaling method, and the characteristic mode analysis are used to describe resonance phenomena.

2.1.1 Electrical Resonance

Electrical resonance is a phenomenon that occurs when an electrical circuit or device vibrates at a specific frequency in response to an external stimulus. This resonance is characterized by a sharp increase in the amplitude of the electrical signal at the resonant frequency, and it can occur in a variety of electrical systems, including RLC circuits, antennas, and micro-electromechanical systems MEMS resonators.
In RLC circuit, for example, electrical resonance occurs when the circuit's inductive and capacitive reactances cancel each other out at a specific frequency, allowing the circuit to resonate [19]. This can be described mathematically using the resonance frequency equation 1:

$$f = \frac{1}{2\pi\sqrt{LC}} \tag{1}$$

where f is the resonance frequency, L is the inductance, and C is the capacitance [19]. The resonance frequency of an LC circuit is the frequency at which the circuit has maximum impedance, meaning that the current passing through the circuit is at its minimum value.
Electrical resonances have many practical applications, such as in electrical systems, as it can be used for filtering, and that's achieved by adjusting the values of the RLC circuit components, the resonant frequency of the circuit can be set to the desired filtered frequency range, enabling the extraction or suppression of specific signals, moreover, it's used for signal processing applications such as tuning the signal into specific range by adjusting the resonance frequency of the circuit [20], another application is in the radio frequency (RF) circuits, where resonant circuits are used to tune RF filters and antennas with a similar concept since a resonator acts as a band-pass filter when an RF signal passes through and passes RF signals at specific frequencies while filtering out unwanted frequencies. .

2.1.2 Mechanical Resonance

Mechanical resonance occurs in physical systems that vibrate or oscillate, such as springs. It occurs when a mechanical system vibrates at a specific frequency in response to an external stimulus. Mechanical resonance occurs when the natural frequency of the system matches the frequency of the external stimulus, the resonance frequency of a mechanical system is the frequency at which the system vibrates with the maximum amplitude, meaning that the displacement of the system is at its maximum value [21]. In a simple mechanical system, such as a mass-spring system, the natural frequency can be described mathematically using the equation 2

$$f = \frac{1}{2\pi}\sqrt{\frac{k}{m}} \tag{2}$$

where f is the resonance frequency, k is the spring constant, and m is the mass of the system [6]. Ultrasound Imaging is an application of mechanical resonance in

medical ultrasound imaging [22]. Ultrasound probes contain piezoelectric elements that vibrate at resonant frequencies, emitting and receiving sound waves used for imaging internal organs and tissues.

2.2 MEMS resonator importance and applications

MEMS resonators are important micro-electro-mechanical systems that have found widespread use in various applications. MEMS resonators are devices that vibrate at a specific frequency enabling them to perform various functions in electronic devices, they are used for sensing, actuation, and frequency reference purposes [23]. The resonant frequency of a MEMS resonator is determined by its geometry, material properties, and fabrication process. In the past decades MEMS silicon resonator usage spread over quartz resonator which is a type of resonant device that utilizes the piezoelectric properties of quartz crystal to generate precise oscillations at a specific frequency, MEMS resonator instead rely on a thin layer of piezoelectric material deposited on a silicon layer to generate the oscillation. The miniaturization of MEMS resonators allows them to be integrated with other microelectronics components on a single chip, resulting in reduced size, weight, and cost. MEMS resonators also offer higher accuracy, stability, and reliability compared to quartz resonators [**?**]. Additionally, MEMS resonator can be easily tuned to specific frequencies by changing their geometry, allowing for customization and flexibility in design.
The energy stored in a system divided by the energy lost per radian is known as a resonator's quality factor (Q). Numerous energy loss mechanisms could be to base for the measured Resonator Quality Factor [24]. Designers are aiming for high Q for many reasons, high quality factor causes resonance characteristics enhancement since a high Q-factor indicates that the resonator can sustain oscillations for a longer duration with minimal energy losses. This leads to sharper resonance peaks and narrower bandwidths, allowing for precise frequency control and better selectivity in filtering applications. Moreover, high Q-factor resonators are more sensitive to changes in the input signal, enabling improved accuracy and resolution in sensing applications.
A novel promising study was published presenting a re-programmable micro-resonator logic gate using a normal industrial design procedure [25]. The device works by employing DC digital inputs to change the resonance frequency of the beam. The proposed design methodology has a considerable potential for increasing energy efficiency and reduces design complexity by 4 to 10 times when compared to conventional CMOS design methodologies.

2.2.1 Timing and Frequency Reference

Researchers have been creating miniaturized, CMOS-compatible, high-quality factor (Q) frequency selection devices using Microelectromechanical Systems (MEMS) technologies for a number of years now in timing and frequency reference circuits [26]. MEMS resonators can be used as oscillators in clocks and other electronic devices that require precise timing. In electronic systems, it is important to maintain

precise timing, and this is often achieved using a quartz crystal resonator. However, MEMS resonators can offer similar performance in a much smaller package, making them ideal for use in portable devices such as smartphones and wearable devices [27]. Moreover, they provide high stability, accuracy, and low power consumption, making them ideal for these applications.

2.2.2 Sensing

MEMS resonators can be used as sensors in a variety of applications, including pressure, temperature [28], and chemical sensing. MEMS resonators can detect changes in resonant frequency due to external stimuli, making them highly sensitive and accurate sensors. When a MEMS resonator is exposed to an external force, it will vibrate at a different frequency, allowing the force to be detected. This can be used in a wide range of sensing applications, from pressure sensors to accelerometers. They can be easily integrated with other sensing components, resulting in highly compact and portable sensing systems. [29] For an example of using MEMS resonator as a temperature sensor, in a recent study [28], research group presented a low-pressure, single-micro resonator, high sensitivity MEMS temperature sensor. Using a temperature-controlled probe station, the device was described. It is highly sensitive, with a resolution of 0.023 °C, and uses only 5 nW of extremely low power. The suggested sensor is also 200–2000 times smaller than the MEMS-based temperature sensors that have previously been shown.

2.2.3 Actuation

MEMS resonators can also be used for actuation purposes, such as in micro-mirrors, micro-pumps, and micro-valves [30]. MEMS resonators can be used to drive these devices with high precision, resulting in improved performance and efficiency. MEMS resonators can also be used as energy harvesters, converting mechanical energy into electrical energy. Another application in the energy harvesting field, they can be used to convert ambient vibrations into electrical energy, and in biotechnology, where they can be used for sensing and drug delivery. Comb drive MEMS resonator has been used for actuation mechanism with a resonance frequency of 15Hz and 24Hz, the study [31] used comb drive which is one of the fundamental models that generates force for capacitive sensors using the electrostatic principle.

2.2.4 Communication

MEMS resonators can also be used in communication systems, including wireless communication and RF circuits [32]. By operating in a very high frequencies, MEMS resonator enables faster data transfer rates and improved communication efficiency. They can be used as filters and resonant circuits in these applications, resulting in improved performance and reduced size and weight. A model has been presented [33] for a (MEMS) resonator that operates at whispering gallery modes (WGMs) and features multiple electrodes for driving and sensing with high Q values. The resonator has two different radii of 37 µm with 53 - 176 MHz and 18 µm with 112 - to

366 MHz. Each mode exhibits Quality factor values over 10000. The multi-electrode configurations allow for the enhancement of specific modes while suppressing others, resulting in a more than 6 dB improvement of the spectrum peak while maintaining high Q values.

2.3 MEMS resonator materials and fabrications

Microfabrication techniques have opened up new paths for the development of nano and micro scale smart sensing devices with improved sensitivity, lower fabrication costs, and relatively low power consumption as a result of technological advancements in micro-electro-mechanical systems (MEMS).
The different material properties, which can be categorized as mechanical, electrical, chemical and thermal are very important for determining the MEMS resonators' optimal degree of performance. Due to the frequent use of these MEMS resonators in harsh environments, it is increasingly important to have understanding in order to eliminate some of the causes of device failure through correct material selection, design, and manufacturing technique [34].
Si-based resonant sensors are among the systems that have been extensively studied. In order to replace the quartz-based resonator, a higher Q-factor component with a smaller form factor MEMS resonator is required in low-phase noise and stable temperature applications [2]. Si has a low thermal expansion coefficient that is, in comparison to steel and aluminum, between 8 and 10 times smaller and has a diamond lattice crystal structure which can exist in all three of its crystalline, poly-crystalline, and amorphous forms. Due to Silicon electrical resistivity, it can be either an insulator or a conductor depending on the situation. Due to all of these characteristics, silicon (Si) is well suited for mechanical, thermal, and electrical device integration, which increases its suitability for extreme environmental applications [35]. The use of single crystalline silicon in resonators is particularly appealing. It can be manufactured in such a way that its material properties are reproducible and well known, and, more critically, it is a very stable material (over time) with very low intrinsic mechanical losses [6].
MEMS resonator can be fabricated utilizing different microfabrication techniques such as surface micro-machining, and bulk micro-machining and (LIGA) technique which is a German abbreviation of (*Lithographie* - Lithography, *Galvanoformung* - Electroforming, *Abformung* - Moulding) [36]. The advantage of constructing MEMS resonators based on silicon-on-insulator (SOI) wafers over micro-machining poly-silicon MEMS resonators is the availability of thicker structural layers. Maintaining low film tension is difficult in poly-silicon while trying to realize dense structures [37]. These days, SOI wafers are also a crucial substrate material for making MEMS devices. A device layer in/on which the devices are produced, a handle wafer that provides mechanical strength during the fabrication process, and a buried oxide (BOX) layer that isolates the device layer from the handle wafer make up SOI wafers [38]. Figure 2 shows the difference between standard SOI, Cavity SOI and cavity BOX.
In a SOI process, the silicon device layer, which is available in a variety of thicknesses,

nearly usually defines the resonator structure. Thicker constructions are preferred for laterally vibrating resonators to reduce motional resistance. In SOI-based resonators, narrow gaps are still required to enhance electromechanical coupling. The method of applying conformal side wall oxide to define the gaps must be changed in order to realize small lateral capacitive gaps in a SOI process.

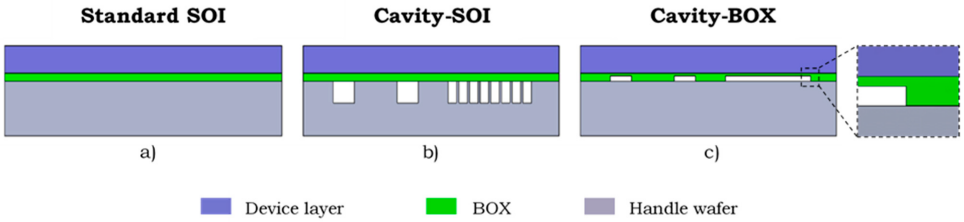

Figure 2: Different architectures of substrate, a) Standard SOI substrate (b) Cavity-SOI substrate with cavities in handle wafer (c) Cavity-BOX substrate. Adopted from [38]

Piezoelectric film is an important layer in the micro-fabrication of the MEMS resonator because of its ability of conversion of mechanical energy into electrical energy, increasing the sensitivity and selectivity of the device. Second, it can improve the stability of the device by reducing the effects of temperature and aging. Finally, it allows for the design of more complex resonator structures, such as multi-mode resonators or arrays, which can have improved performance over single-mode resonators. Materials with greater piezoelectric coupling coefficients, such as lithium niobate (LiNbO3) are used in different designs [39], in an effort to achieve larger coupling coefficients in the pursuit of developing low insertion filters based on laterally vibrating resonators. Since the material cannot be deposited as a thin film, the procedure is different from the depositing AlN for instance. When compared to AlN resonators, MEMS resonators made of LiNbO3 have been demonstrated to have substantially reduced insertion losses.

2.4 Resonance modes

Resonance modes are a fundamental aspect of systems where resonance occurs. Resonance modes refer to the distinct vibration patterns or modes of oscillation that can occur in a resonant system associated with specific frequencies. These modes can be characterized by the number and positions of nodes and antinodes in the system, representing regions of maximum and minimum displacement.
The specific resonance modes that can be excited in a MEMS resonator depend on the shape and material properties of the resonator. These will be somewhat influenced by the way the beam is supported, where it is supported, and where the vibration is driven or excited by striking. Different resonance modes can be designed into a MEMS resonator, and that will result in characteristics variances such as power handling capability and spurious modes presence [6].

2.4.1 Bulk mode

Bulk mode resonators exhibit structural deformation as a result of planar contractions or expansions. The resonant frequencies of bulk modes mainly depend on the lateral physical dimensions of the structure, such as width or length, in terms of geometrical dependence. Length extensional (LE) and width extensional (WE) are forms of the bulk resonance modes, where longitudinal modes is particularly important in MEMS resonators because they are often the most efficient modes for sensing and actuation [37]. An example for using LE resonator will be presented in this thesis as the main design. Figure 3 shows how the width extension deforms the resonator while figure 4 shows the direction of deformation in the length extension mode case.

2.4.2 Flexural mode

The bending of the structure along its length, causing motion in the transverse direction perpendicular to the length, is a characteristic of flexural mode vibrations [37]. Beam and plate constructions can both induce flexural modes. The flexural mode, in particular, has a high sensitivity to changes in the environment, making it well-suited for sensing applications. Figures 5 illustrates the flexural modes in a beam with different boundary conditions simulated using ANSYS software 2021 R2 (Ansys Inc., United Stated) where in figure 5.a the fixed boundary condition at both ends, hence, the beam is deflected form the center and in 5.b the beam is fixed from one end while the other end is free and can be deflected.

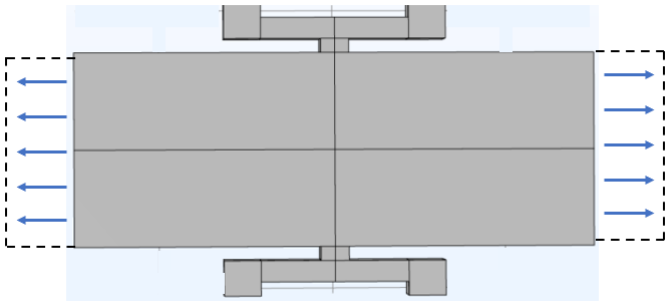

Figure 3: Width extension (WE) mode, arrows show the direction of the beam deformation

2.4.3 Coupled resonant mode

Coupled resonant modes refer to the phenomenon of multiple resonant modes in a MEMS resonator that are coupled to each other through mechanical or electrical interactions. The number of modes that can exist in an array grows as the array size does, presuming that each resonator has the same vibration mode. The frequency separation between the modes widens if the resonators are closely connected to one another. By assembling arrays of the same resonator that are synchronized to vibrate

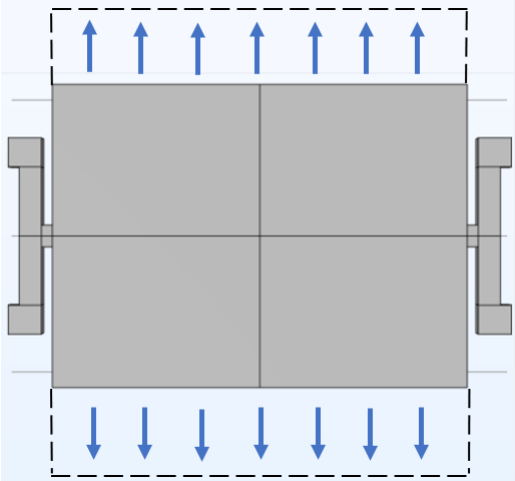

Figure 4: Length extension (LE) mode, arrows show the direction of the beam deformation

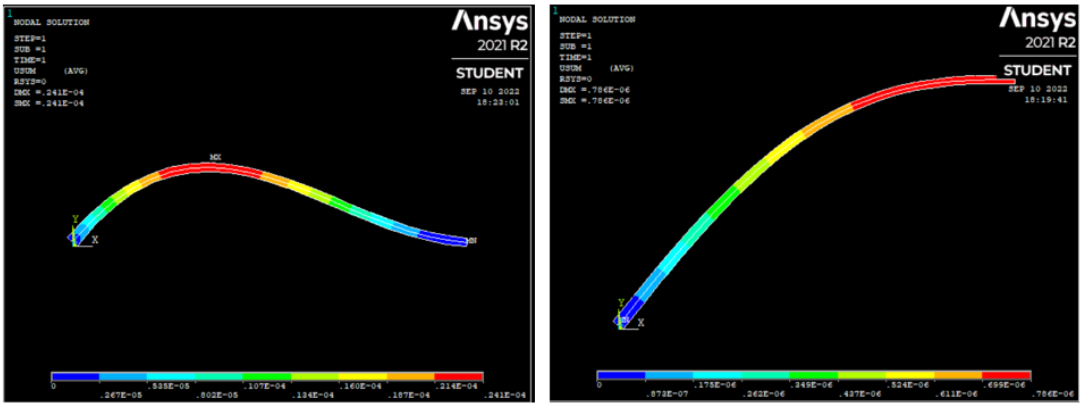

(a) (b)

Figure 5: (a) Flexural mode in clamped-clamped beam where fixed boundary at both ends.(b) Flexural mode in a cantilever where fixed boundary at one end, simulated using ANSYS mechanical APDL software

at the same frequency, this method is very effective for boosting the output signal intensity of MEMS resonators [40]. This is especially helpful in reducing the phase noise of MEMS oscillators and the insertion loss of filters [41].
Coupled resonant modes have several uses in MEMS resonators. One example is the creation of multi-frequency resonators that can operate at multiple frequencies simultaneously. By designing the resonator structure and the coupling between the modes appropriately, it is possible to excite multiple modes with high quality factors within a single device. This can be useful for applications such as multi-band filters, where a single device is required to filter multiple frequency bands [42] .
Another application of coupled resonant modes is in sensing and actuation. The capability for common mode rejection because of the differential structure. These

benefits have made it possible for novel sensors with unmatched sensitivity [42]. A MEMS resonator can be designed such that one mode is sensitive to a specific physical parameter, such as temperature or pressure, while another mode is used for actuation. By coupling the two modes, it is possible to create a highly sensitive and selective sensor that can detect small changes in the physical parameter of interest.

2.5 Role of microfabrication on MEMS resonator quality

The small-scale properties of high frequency resonators, which are strongly influenced by sub-micron size fluctuations, make their fabrication difficult [43]. After the fabrication process, the micro devices that do not interface with the environment can be completely enclosed. MEMS resonators are often packaged on two levels: wafer level and conventional packaging. To prevent mechanical movement, a resonator must be retained in the cavity. When the resonator is not hermetically sealed, the stability of the resonance frequency reduces [44] [45]. The introduction of failure to the MEMS resonator is caused by structure adhesion to the system and poor tribological performance, which can be improved by chemical and tribological surface modification, thin and dual-film coating, etc. The MEMS resonator's performance and consistency are greatly enhanced by testing. However, device testing consumes up to 35% of the total production cost, therefore the fabrication of MEMS resonators necessitates intense work and extensive research knowledge. Failures in MEMS resonators can be brought on by sticking, a bad ecological condition, static overload, fatigue, and other factors [**?**]. It is discovered that the two main manufacturing concerns, which frequently result in short circuit problems for MEMS devices with refilling isolation trenches, are silicon residue at the terminal of the trench and metal stringers along indentation on trench surface. The two nearby structures, which are intended to be electrically insulated, will have a short circuit problem as a result of the residual silicon. In order to address this issue, the DRIE process has been adjusted to provide reentered profiles with decreased top and bottom widths. An issue occurred with the fabrication of the MEMS resonator of being short circuit, it is discussed by Xie et al. [46] study, the issue arises because of Si residue is present along the terminal-trench, and metal stringers are present along the trench surface. Residual-stresses, electrical static forces are all responsible for stiction-related failures in the resonator. However, the study proposed solutions by preparing a hydrophobic surface, reducing the contact area, and lowering adhesion.
For introducing new fabrication technique that is more robust for piezoelectric MEMS resonator, a recent study introduced a laser micromachining technique that can be a substitution for the traditional micromachining techniques [47]. The main goal of the new fabrication flow is to use less of the conventional microfabrication technology in order to decrease process complexity and turnaround time. Traditional micromachining techniques iterate or repeat a three-step cycle. Layer by layer, materials are indirectly treated. Material deposition is done first, then masking lithography. The deposited material is selectively etched as the final stage. The traditional process is very accurate although it's difficult. However, it is the only reliable method for processing silicon materials at a large scale, creating the framework for silicon MEMS

device and integrated circuit microfabrication operations. Contrarily, the situation with polymeric materials is different. In addition to layer-by-layer micromachining flows based on the 3-step cycle, direct patterning techniques can be used to produce polymeric microstructures. Because these direct processing technologies do not require masking lithography or selective etching, the complexity of the entire process is greatly reduced. 3D printing and laser micromachining are typical examples of polymer direct processing methods.
A study group used the Zinc oxide as a piezoelectric material since it can be deposited at lower temperature, which can reduce the thermal fabrication cost and for the ZnO's superior bio-compatibility and biodegradability that could be helpful in resonators used as mass/pressure detectors in medical applications [48]. Two-level electron beam and two-level optical lithography were used to fabricate the resonators. The resonator had a quality factor of 220 and an 882 MHz resonance frequency.

2.6 MEMS devices defects formation

2.6.1 Testing induced defects

MEMS devices are subjected to different kinds of tests, those tests can be destructive or non-destructive and they carried out to test different properties of MEMS devices such as the robustness, electrical response and many other properties. Tape peeling method is a testing technique used in MEMS devices to evaluate the adhesion strength between different layers or interfaces within the device [49]. It involves the controlled application and removal of adhesive tape to assess the integrity and reliability of MEMS structures. The tape peeling method typically starts by applying a layer of adhesive tape to the surface of interest. The tape is carefully pressed onto the device to ensure good contact. Then comes the peeling step when The tape is then peeled off the surface in a controlled manner. The peeling process can be performed manually or using specialized equipment, depending on the specific requirements and desired accuracy. After peeling, the condition of the tape and the device surface is examined [50]. The evaluation may include visual inspection, microscopic examination, or other techniques to assess the presence of any delamination, damage, or residue on the device surface.
By analyzing the condition of the peeled tape and the device surface, the tape peeling method can provide insights into the adhesion quality and potential issues within the MEMS device. It helps to identify regions of weak adhesion, delamination, or potential reliability concerns that may affect the device's performance or longevity. For other purposes, tape peeling method can be used to check the vulnerability of some parts to crack or detach, further in this work, tape peeling method will be used to induce defects for the weak parts of MEMS resonator.

2.6.2 Operational defects

Other than the intentionally desired modes, MEMS resonators can exhibit spurious modes, which are additional unwanted resonant modes that can interfere with the desired resonant mode of operation. Spurious modes can have detrimental effects on

the performance and reliability of MEMS resonators [51]. These modes can occur due to various factors such as structural asymmetries, imperfections in fabrication, coupling with surrounding structures, and parasitic effects. They can overlap with the desired operating frequency of the MEMS resonator, leading to frequency interference and distortion of the resonator's response [52]. This interference can affect the resonator's frequency stability, accuracy, and overall performance. Spurious modes often have different mode shapes compared to the desired mode. These variations can result in non-uniform stress distribution, which can lead to mechanical stress concentrations and potential reliability issues, including fatigue and failure of the resonator.
In this work, spurious modes were used as a main source of inducing cracks, by applying electrical signal for specific spurious modes to mimic the operational behaviour of MEMS resonator.

2.7 MEMS devices defects detection

The architectures of micro-electro mechanical system (MEMS) components are incredibly precise, and visual examination with a lot of labor is often used to ensure their quality control. The manual detection method has inconsistent quality issues due to its inefficiency (poor yield) and reliance on each person's unique capacity for visual discrimination. Furthermore, human inspection can hardly meet the 100% overall inspection criterion for key items, hence, the automated defects detect ions techniques have been widely used, the automation offers a high rate of recognition and improves detection efficiency for QC practical industry objectives, making it a crucial important technology in current advances. Because MEMS architectures are so intricate, manufactured parts frequently have flaws including cracks, scratches, particles [53]. According to the application and the needs of the detection method, the techniques is determined, those techniques can be optical detection method, infra-red IR imaging, scanning electron microscope (SEM), and electrical methods by testing the device performance electrically.

2.7.1 Automated optical inspection (AOI)

Automated optical inspection (AOI) system is an integrated systems consists of hardware and software components used for different purposes, varies from measurement, inspection and classification to process monitoring and object positioning. The capabilities of the systems can be adjusted to meet the application needs such as the software accuracy and run time, hardware speed and camera resolution. Defects and defect patterns can be found using AOI. The root causes of element failure can be found with the aid of AOI too [54]. The method of defect identification has as its first hurdle the discovery of the defect itself. Different light sources and illumination methods are employed to solve this issue [55].
The movement of the AOI system stage can produce vibration noise, to overcome this problem S. Pan and K. Chen [56] designed a stage for AOI systems motion-induced vibration suppression. In the mentioned study, a test stage made of compliant

structure and elastomeric bearings were used as shown in figure 6. The efficiency of motion-induced vibration suppression was initially assessed using both input shaping and loop transmission shaping techniques. According to the positioning control results, it was possible to obtain a 0.5% overshoot, a 0.09 second setting time. Another application for AOI systems was mentioned in Chen, P.-C. research [57],

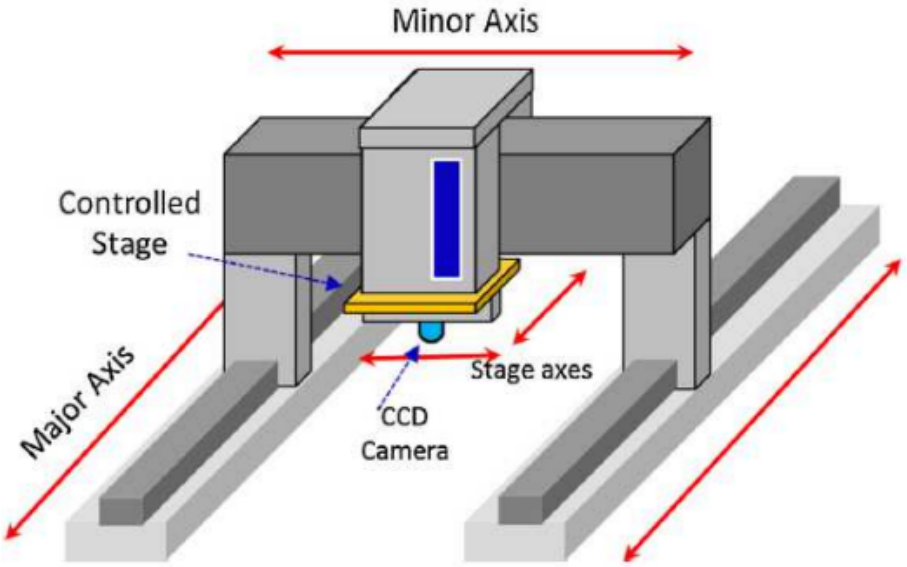

Figure 6: AOI 3-axis stage using elastomeric bearings for vibrational noise exclusion. Adopted from [56]

where the objective of the work was to create an automated optical inspection (AOI) system that can quickly and accurately assess the size of microchannels placed inside a transparent polymeric substrate. Snell's law forms the basis of how the AOI system was built. The idea states that when light travels through two transparent media (air and the transparent material of the microfluidic chip), the cross-sectional dimensions of the microchannel can be determined by analyzing the parallel refracted light from a light source that passed through the microchannel using formulas derived from Snell's law.

2.7.2 Electrical testing

Different steps of the manufacturing process for MEMS devices include testing. This testing is necessary to confirm the device's parametric and functional performance parameters. MEMS are checked by measuring all AC and DC parameters at the wafer level after wafer level manufacture. This can be done manually or using an ATE (Automatic Test Equipment). By utilizing circuitry that is designed for testability within the chip, this test phase separates the wafer for good and faulty die [58]. In this test method, a physical signal, such as an electrostatic force, is produced inside the MEMS by an electrical signal. Key functional sub-structures of the MEMS are

anticipated to respond to this physical signal by acting in some way [59].
In MEMS resonator, AC signal is subjected on the resonator in order to check the frequency response of the device, the response can indicates if the device is defected or not, although, a specific test recipe should be applied in order to test the electrical response by identifying the frequency and power will be used to test the device. The resonance frequency peak can be one of the ways to test the robustness of the resonator, however, it will not be successful way sometimes unless the device is majorly defected, moreover, it can be faultily mixed with poor resonator design. On the other hand the use of parasitic modes can be a good way of identifying the defects. In figure 7.a and 7.b the resonance peak has no major difference between the robust resonator and defected resonator with the different power used to activate the device, however the difference in the parasitic peaks in figure 7.c and 7.d is obvious specially with using high power.

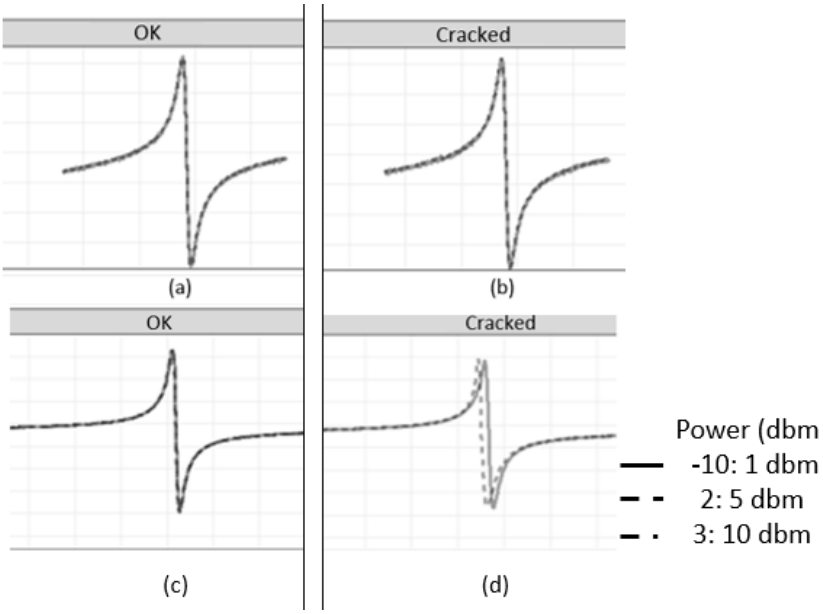

Figure 7: Nearly identical resonance peaks in (a) robust resonator and (b) defected resonator, on the contrary the difference appears between specific parasitic peaks in (c) robust resonator and (d) defected resonator, the difference can be noticed with using 2: 5 dbm and 3: 10 dbm power sweeps

3 Research material and methods

Different test designs were implemented in order to examine the robustness of the resonator and study the possible defects and cracks formation in different fabrication and operation stages, moreover, validating the results of the detection methods used to inspect those defects. Different considerations were taken with those designs such as:

1. Different anchor shapes to check the geometry effect on the defects formation.
2. Different spring dimensions to achieve different spring stiffness.
3. High quality factor Q.
4. Different beam widths with a maximum value of 290 µm considering the cavity size in which the resonator will be processed.

Those design were simulated using COMSOL Multiphysics software 6.1 (COMSOL AB, Sweden) [60] and MATLAB 2022b (MathWorks, United States) [61].

3.1 MEMS resonator design

3.1.1 MEMS resonator dimensions and anchor design

For this thesis work, different designs have been implemented to study the cracks of the MEMS resonator, 32MHz and 24MHz are the main designs will be discussed in this work in order to accomplish better alignment with KTO market needs.
Resonator length in the (LE) mode is the factor specifying the resonance frequency, hence, the length for each specific frequency will remain constant while the resonator width will be swept. Figure 8 shows the design of the resonator used which is a clamped-clamped single beam, figure 9 shows the different anchor shapes used in the study, and the two main dimensions swept for different designs which are the spring length and the spring width.
The designs layouts were implemented using Klayout software 0.27.8 (Klayout, Germany) and MATLAB scripting and imported into COMSOL Multiphysics software to implement the Finite Element Method (FEM) simulations. Figure 10 shows the FEM simulation of the main LE modes of 2 different 24MHz resonators.

3.1.2 Quality factor optimization

For the enhancement of resonance characteristics and minimizing the energy loss within the device, as mentioned in 2.2, different parameters were swept in order to reach a high quality factor for the MEMS resonator test designs, such as:

1. MEMS resonator beam width.
2. Anchor spring length.
3. Anchor spring width.

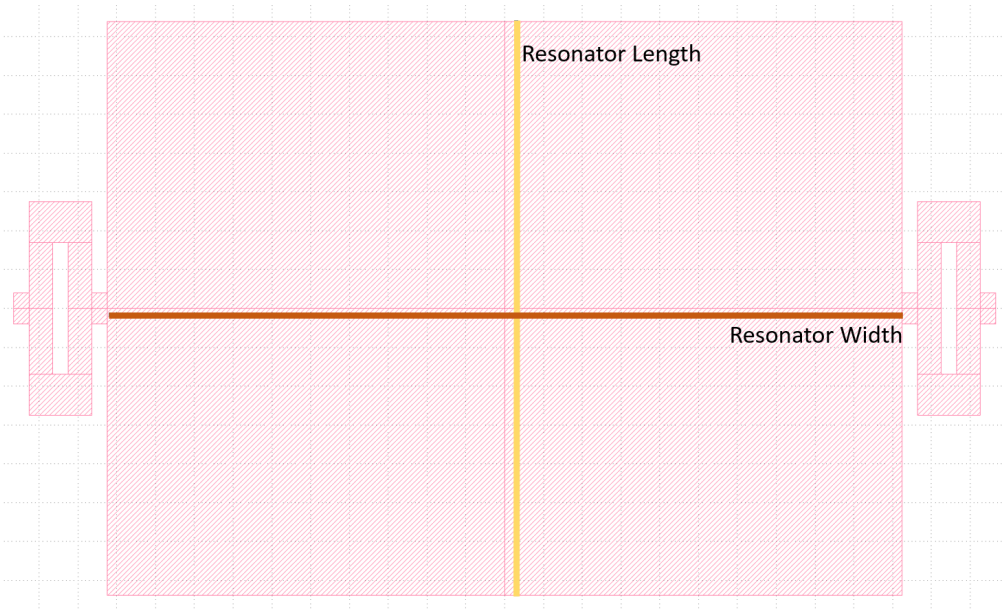

Figure 8: Resonator structure, a clamped-clamped rigid beam with a folded spring anchor shape

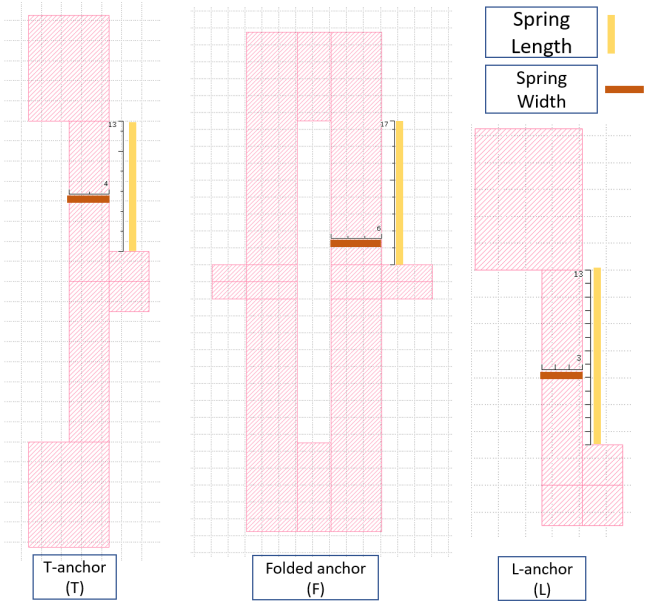

Figure 9: T-shape, Folded spring shape and L-shape anchor designs

4. AlN piezoelectric layer thickness.

Figure 11 shows the result of sweeping 24-MHz resonator beam widths as in the x-axis, y-axis showing the quality factor for the corresponding width, different line colors showing the different anchors shape where L is L-shape anchor, T is the T-shape anchor and F is the folded spring anchor. AlN thickness effect was tested

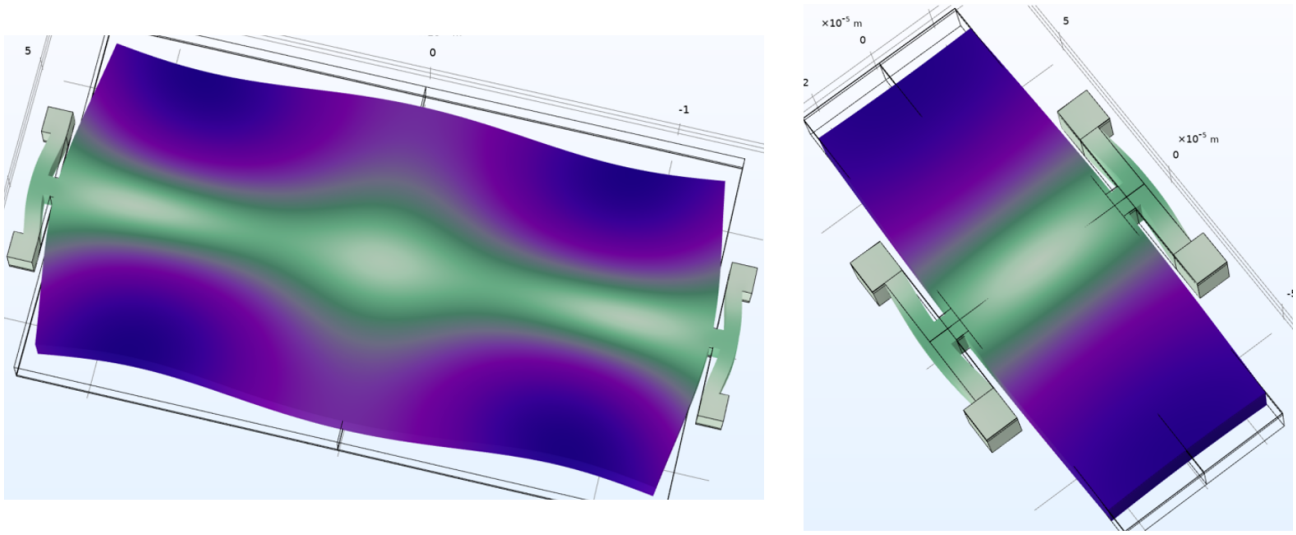

(a) (b)

Figure 10: Main mode shape for (a) T-anchor, resonator beam width of 200 µm. (b) T-anchor, resonator beam width of 50 µm.

as well where each graph of the 3-panel graph shows different AlN thickness. The same analogy is shown in figure 12 although it shows the sweeping results of 32-MHz resonator.

In order to check the effect of the spring length and spring width, different values were simulated with the sweep of the beam width as shown in figure 13, where 2 values of 6 and 8 µm spring width were simulated, with 4 different spring length values (9, 13, 17 and 21) µm for a T-shape anchor 32-MHz resonator. For L-shape and folded anchor, another sweep can be found in figure 14 which shows the quality factor values against the beam width, using 17 µm spring length and 6, 8 µm spring width.

AlN layer thickness effect on the quality factor was studies with using 1.45 µm and 1.475 µm layer thickness with sweeping of resonator beam width, figure 15 shows the values of Q against beam width for different AlN thicknesses.

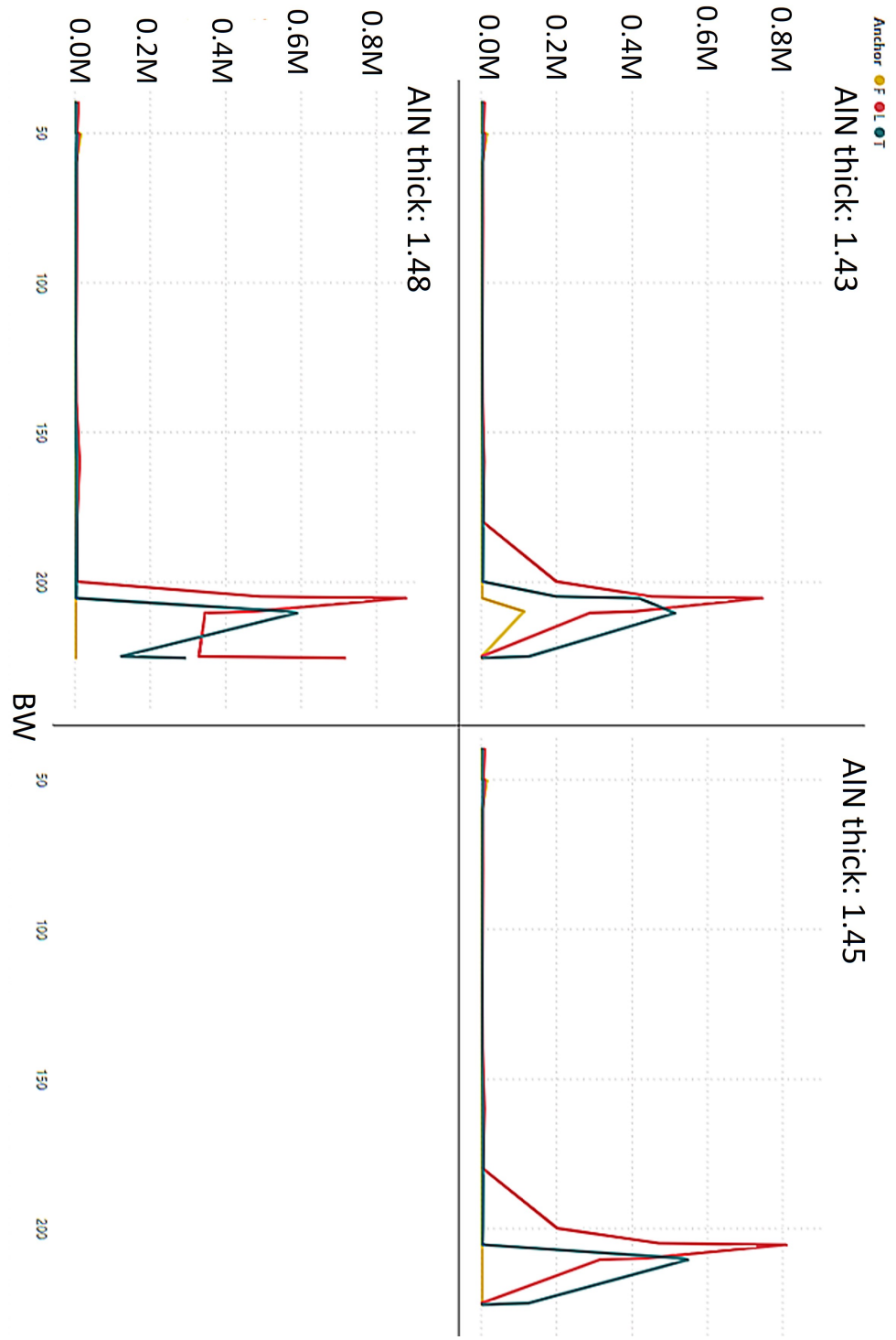

Figure 11: Optimization the Q-factor for 24MHz resonator design, Q-factor vs beam width. Different line colors represent the different anchor shape (L-anchor, T-anchor and F-anchor), different panels represent different AlN thickness

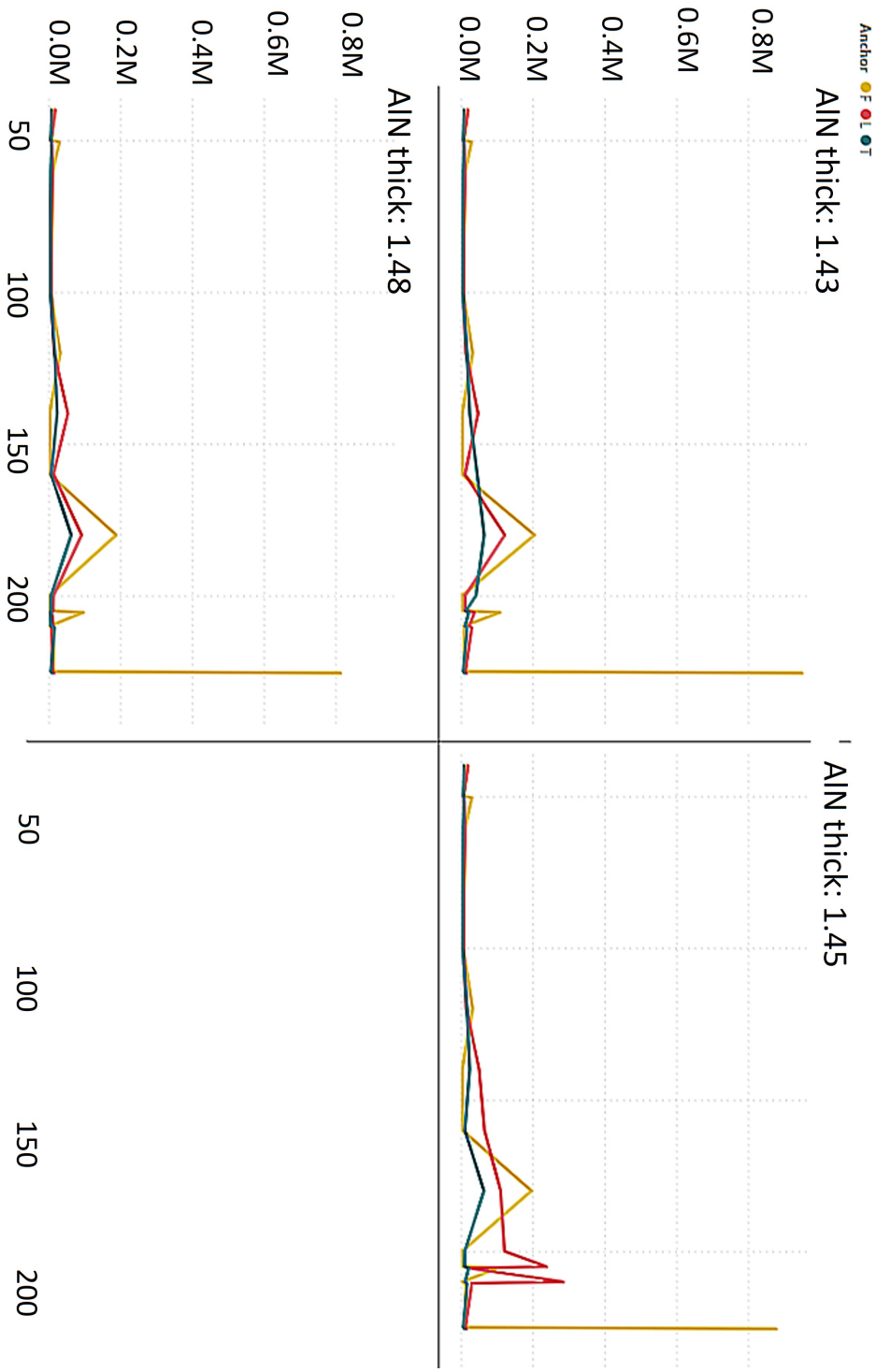

Figure 12: Optimization the Q-factor for 32MHz resonator design, Q-factor vs beam width. Different line colors represent the different anchor shape (L-anchor, T-anchor and F-anchor), different panels represent different AlN thickness

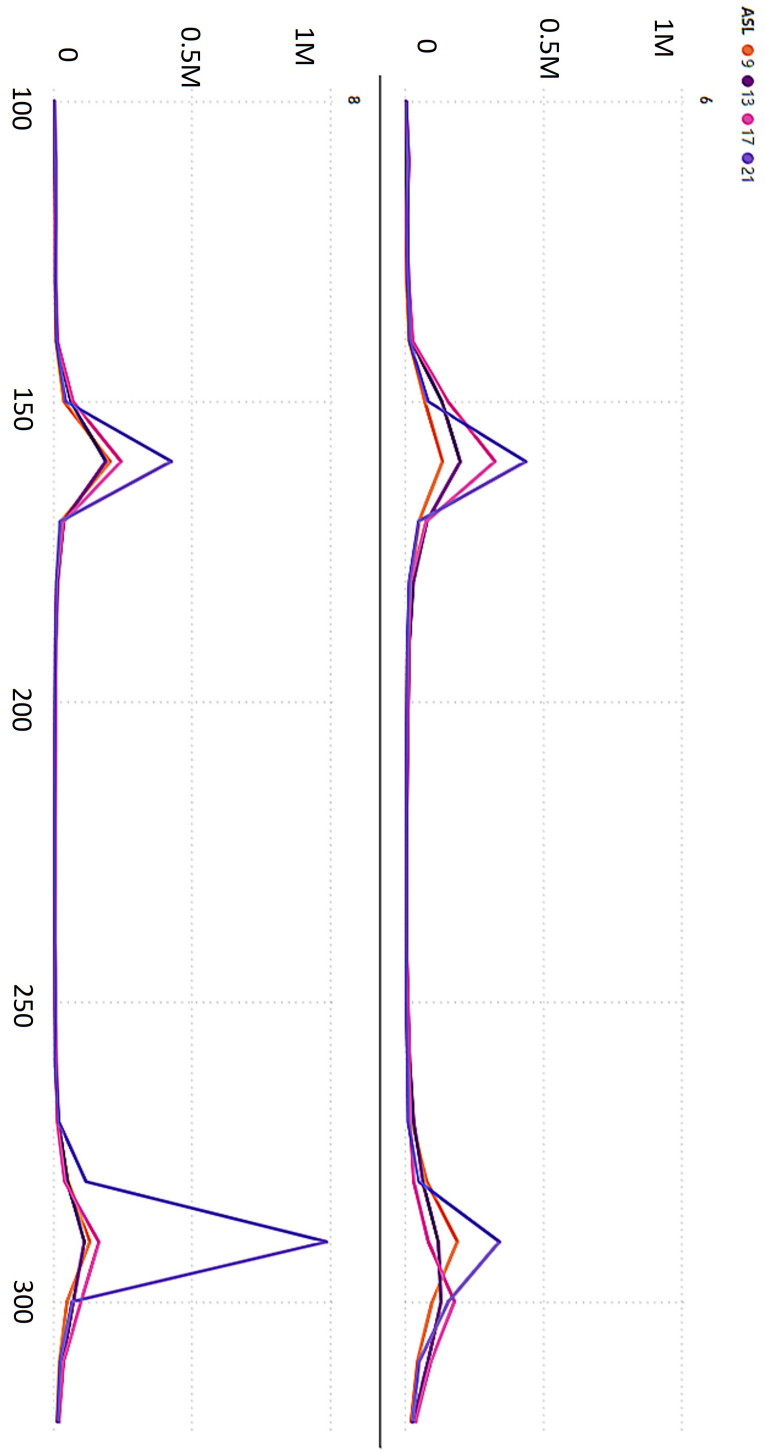

Figure 13: Q-factor vs beam width, different line colors represent different spring length, the two panels represent different spring width values

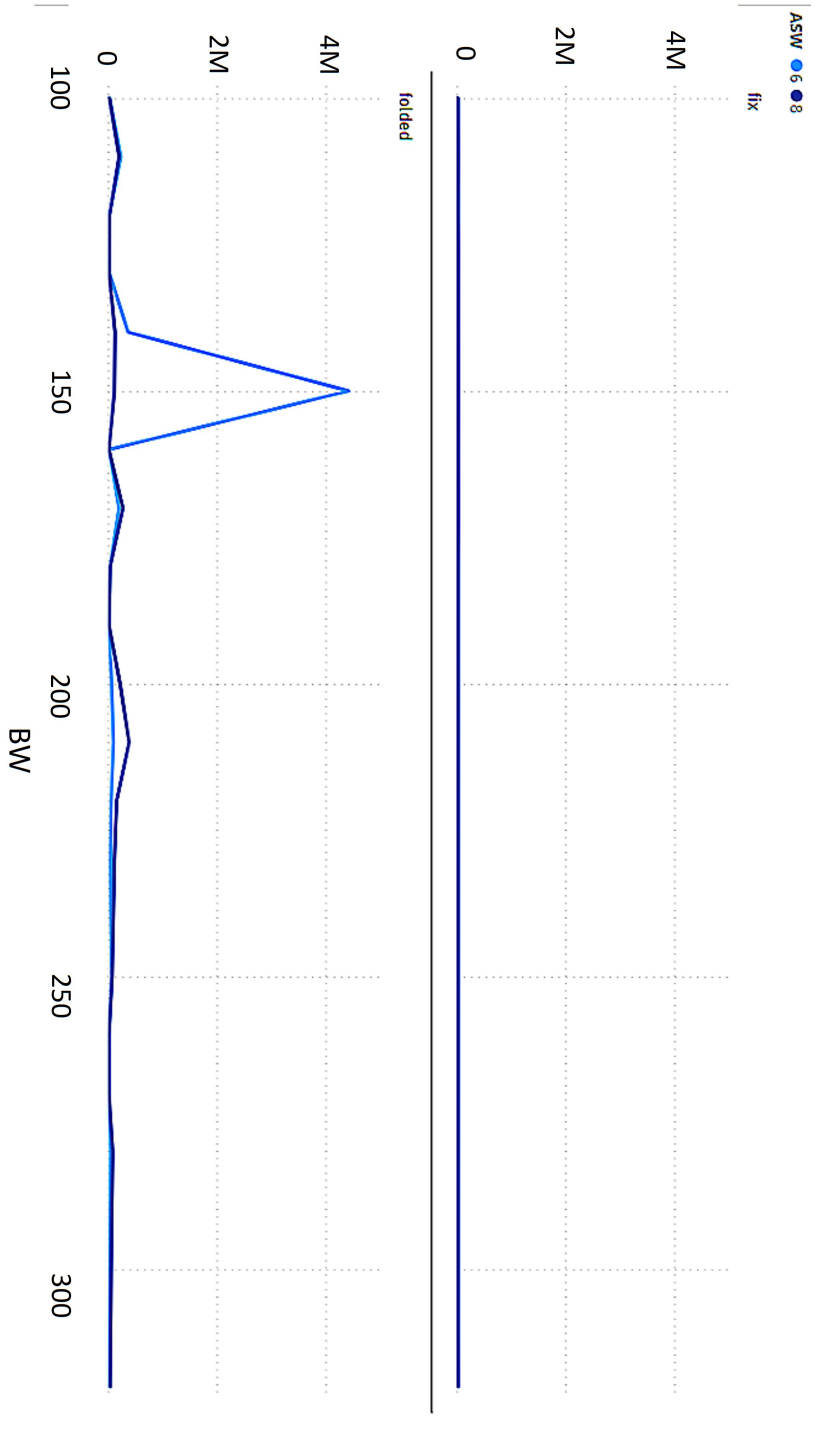

Figure 14: Q-factor vs beam width, different line colors represent different spring width, the two panels represent different anchor shapes (L-anchor and F-anchor)

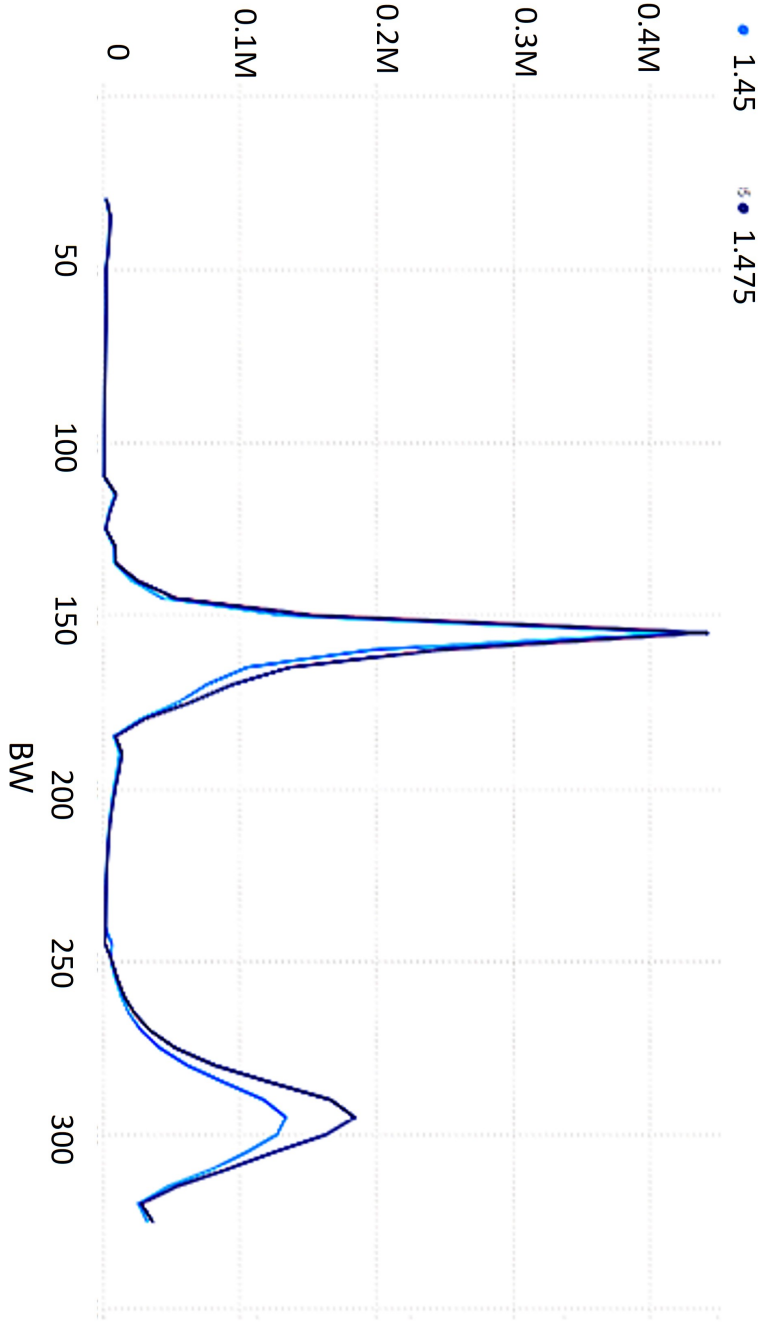

Figure 15: Q-factor vs beam width, different line colors represent different AlN thicknesses

3.1.3 Spurious mode analysis

Part of the defects can be formed during the operation of the resonator, as discussed in 2.6.2, spurious mode can be a main cause of defect for resonators depending on the mode shape, hence, to check the robustness of the designed devices the spurious mode shapes were studied to detect which mode shape resonance would cause the highest risk on the resonator, figure 16 shows all the spurious peaks in a T-anchor of 32-MHz resonator as a frequency vs admittance graph, the spurious mode shapes of those peaks were simulated using COMSOL software. Figure 17 illustrates the mode shapes of a the specified peaks in figure 16.

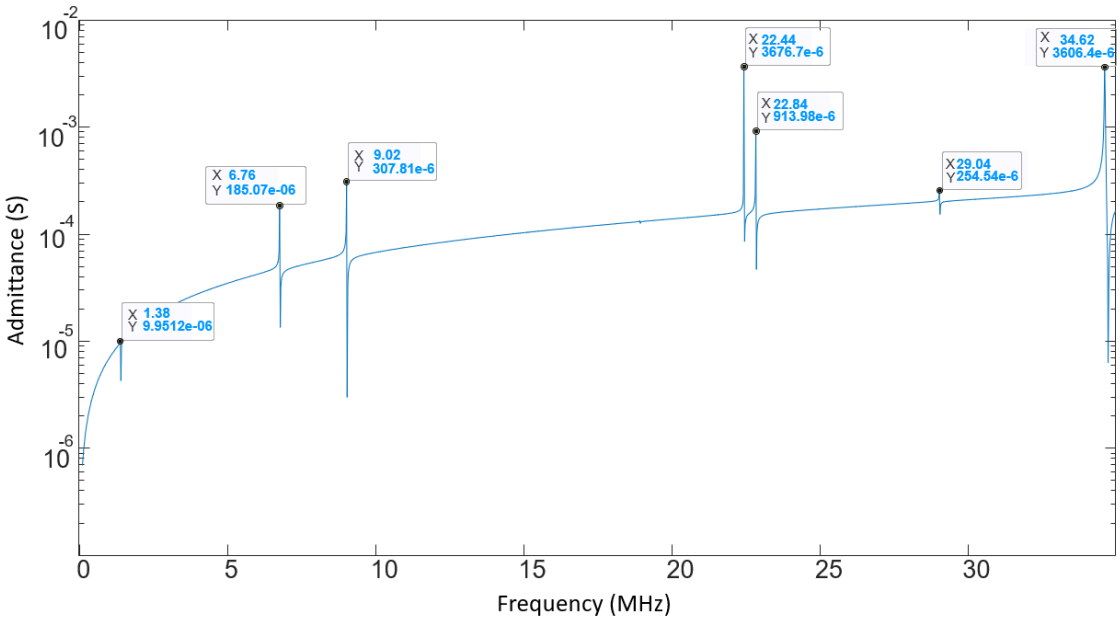

Figure 16: Spurious modes frequency peaks for a T-anchor, 150 µm resonator beam width, 32-MHz resonator

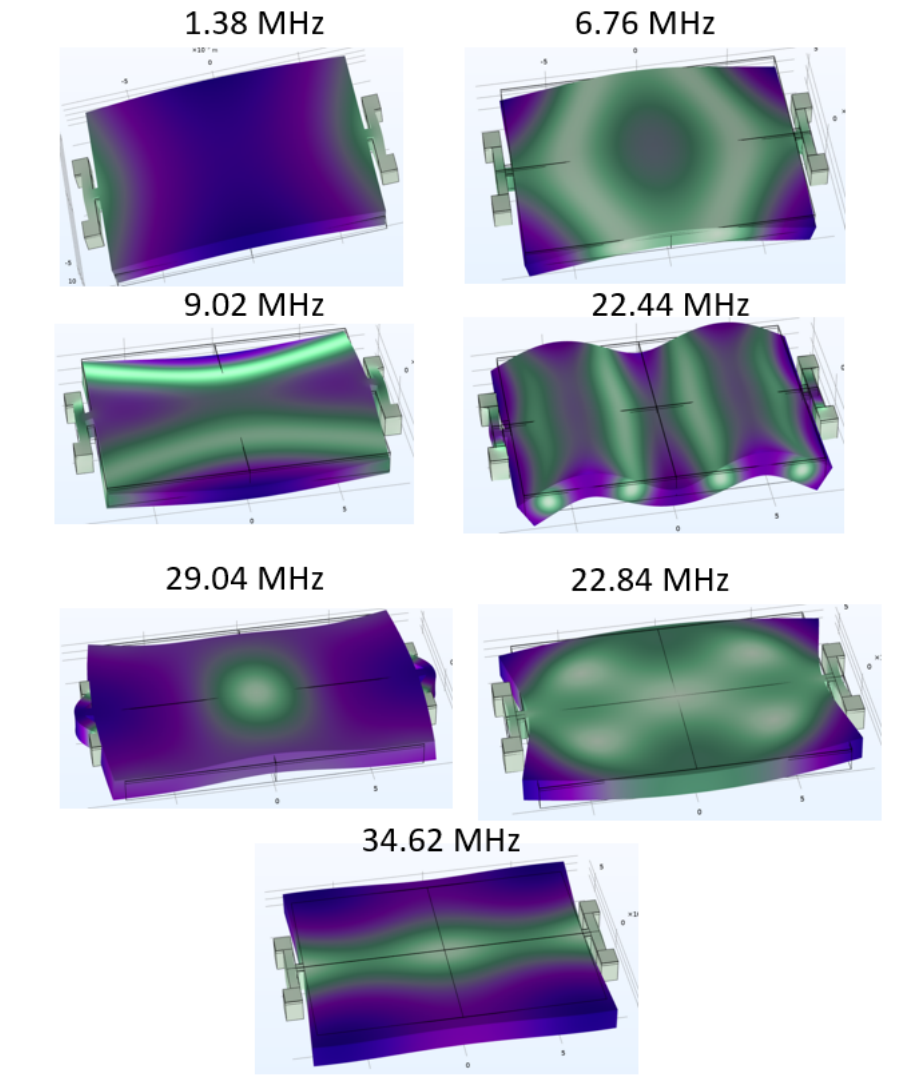

Figure 17: FEM simulations for spurious modes shapes for a T-anchor, 150 µm resonator beam width, 32-MHz resonator

3.2 Defects inducing

3.2.1 Electrical inducing

To test the robustness of the different designs, some defects were subjected to electrical signal aiming to induce some defects electrically, Olvaldi probe station shown in figure 18 and E5100 vectorial network analyzer (VNA) tool shown in figure 19 were used. Using E5100 VNA, specific frequencies were supplied to MEMS resonator, those frequencies were selected as they are suspected to induce defects in the device according to the FEM simulations mode shapes as mentioned in section 3.1.3, moreover, supplied power was controlled and swept from -20 to 20 dbm.

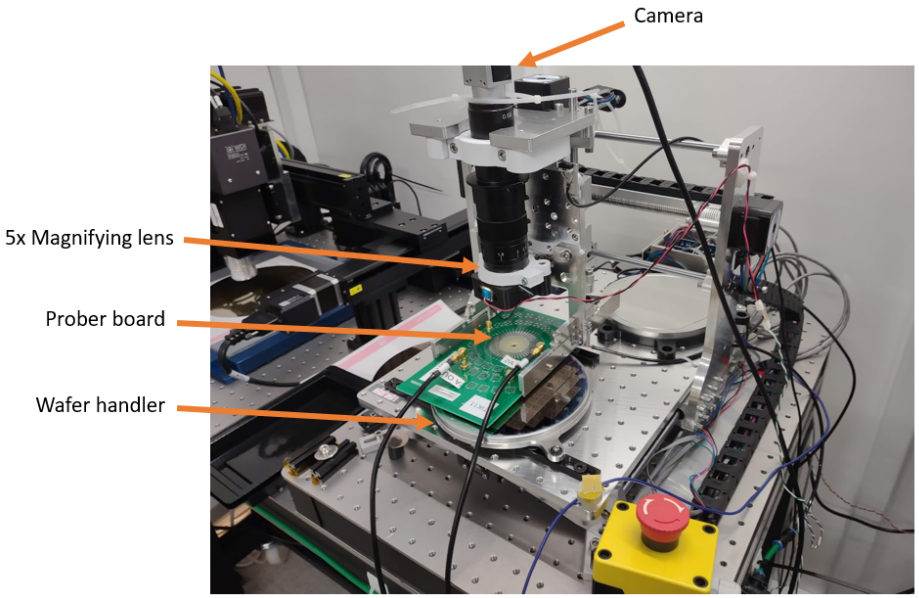

Figure 18: Alshain Olvaldi probing station setup

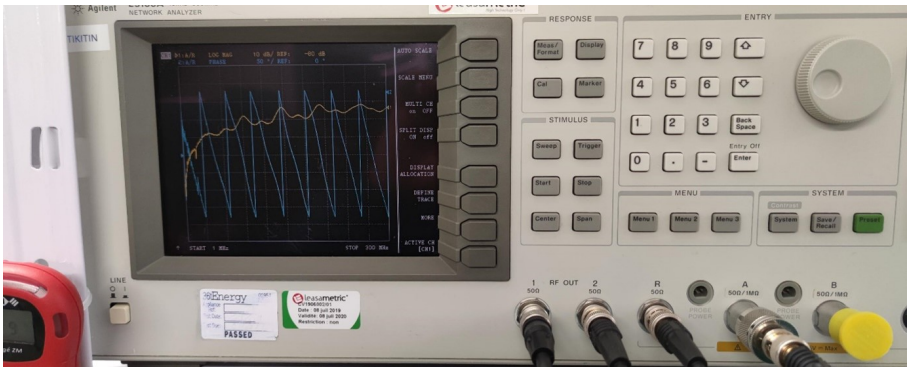

Figure 19: E5100 vectorial network analyzer device

3.2.2 Tape peeling test

Another common robustness test is the tape peeling test 2.6.1, tape peeling was performed to examine the robustness of the different designs, by checking which structure and dimensions were affected the most. Tape peeling was performed to the whole silicon wafer, steps done for the test were:

1. Cover the wafer with ADWILL D-867 tape.
2. Use the ultraviolet curing system with a dose of 735 mJ/cm^2 for 3-scans.
3. Peel the tape manually with a diagonal movement.

3.3 Defects inspection

3.3.1 Optical inspection

For enhanced experience of defects detection AOI system aiming for time reduction and higher detection rate 2.7.1, this study used KTO automated optical inspection tool that developed as a part of this work during the study, the developed AOI tool can be mainly divided into two main stages, as shown in the figure 20, which are the image collection stage and image analysis stage. In the image collection, a hardware tool was set to automate the process of taking the images of the devices on one silicon wafer, an image of the setup is shown in figure 21. The hardware consists of:

1. Wafer handler.
2. 3-axis movement stage.
3. 10x magnifying lens.
4. Camera.
5. Bright and dark field LEDs.

The microscope computer fetches the wafer data from the database to be able to locate the dies in the wafer, then it controls the hardware using Python script by which the lightning and movement can be controlled and the images can be taken. The microscope computer sends the images to the image computer where the needed analysis is done for the images. Using a Python script the images of the MEMS resonator are decided to be robust or defected, these results are then inserted into the database as a reference to the specified wafer.

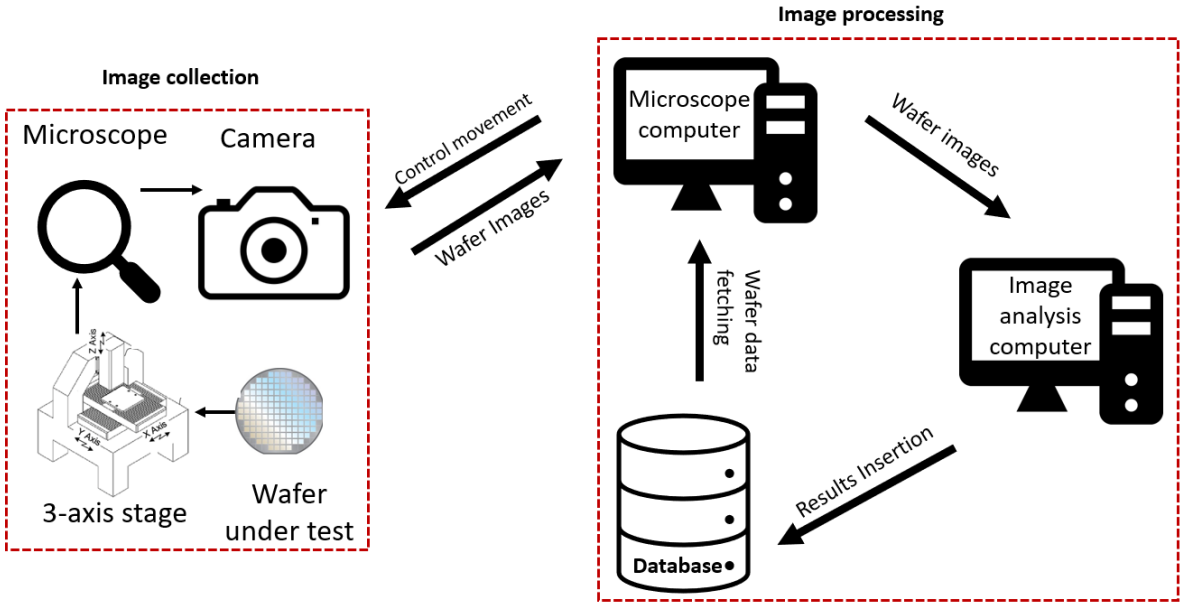

Figure 20: AOI components and the interactions between the two main part of image collection and image analysis

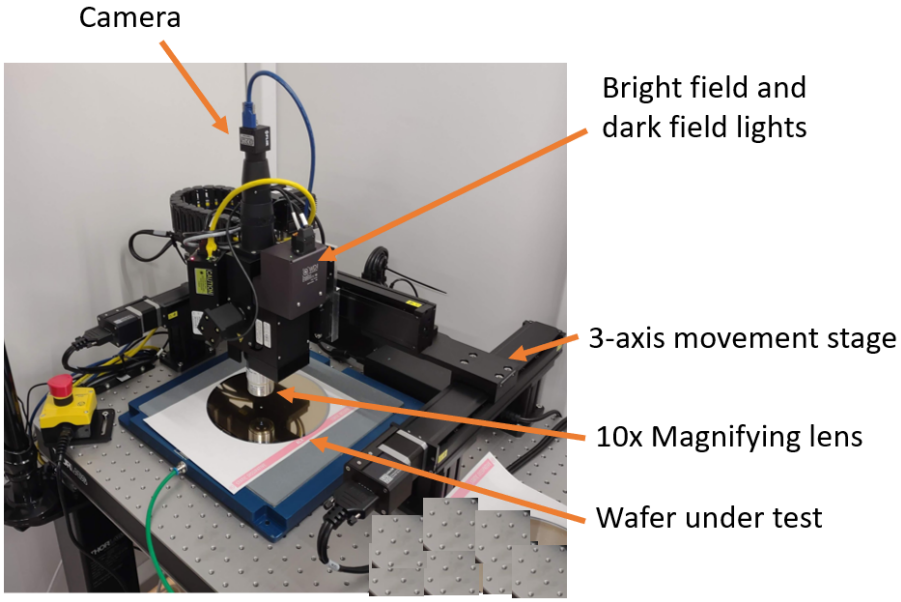

Figure 21: AOI hardware setup

4 Results

4.1 MEMS resonator design

4.1.1 24-MHz resonators

Table 1 contains the dimensions of the implemented designs of the 24-MHz resonator, considering a high quality factor and different anchors spring length and spring width dimensions.
Figures 22 and 23 show the peaks for the spurious mode present in the 24-MHz design, the graphs represent a relationship between the frequency and admittance.

Design number	Anchor type	Resonator width	spring length	spring width
1	L	210	17	6
2	F	210	17	6
3	T	210	17	6
4	L	210	17	4
5	T	200	21	4

Table 1: Specifications of the implemented designs of 24-MHz resonator

4.1.2 32-MHz resonators

Table 2 contains the dimensions of the implemented designs of the 32-MHz resonator, considering a high quality factor and different anchors dimensions.
Figures 24 and 25 show the peaks for the spurious mode present in the 32-MHz design, the graphs represent a relationship between the frequency and admittance.

Design number	Anchor type	Resonator width	spring length	spring width
1	F	140	17	6
2	F	150	21	6
3	F	290	21	8
4	T	150	13	5
5	T	160	17	3
6	T	170	15	3

Table 2: Specifications of the implemented designs of 32-MHz resonator

Figure 26 shows the spurious mode shapes simulations which are presumed to make the strongest effect on the fragile part of the anchor. The figure shows the selected spurious shapes for the three different designs of anchors, these mode shapes are present in all different 24-MHz and 32-MHz designs with different frequency and admittance values.

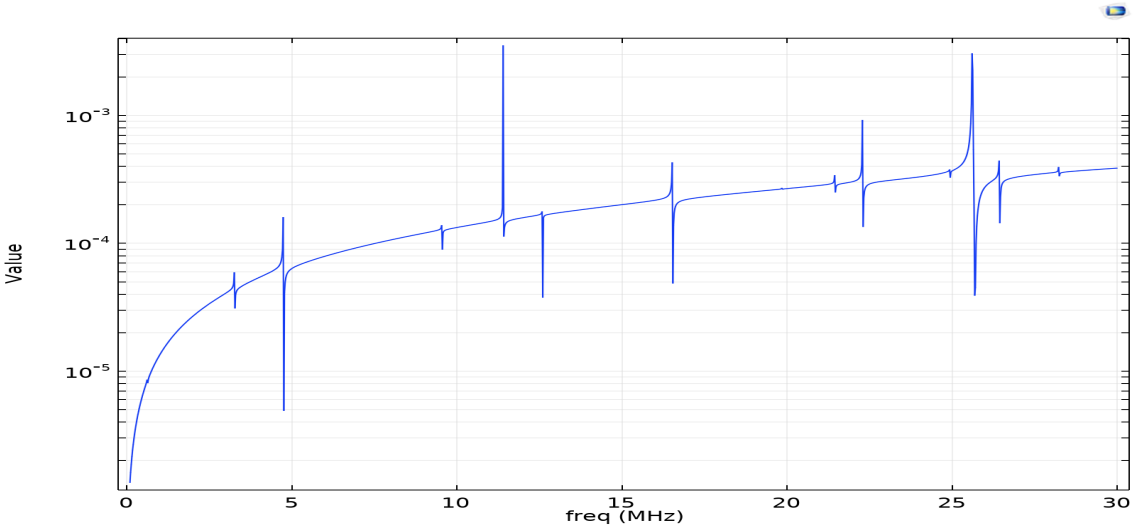

(a) 210 µm beam width, folded anchor

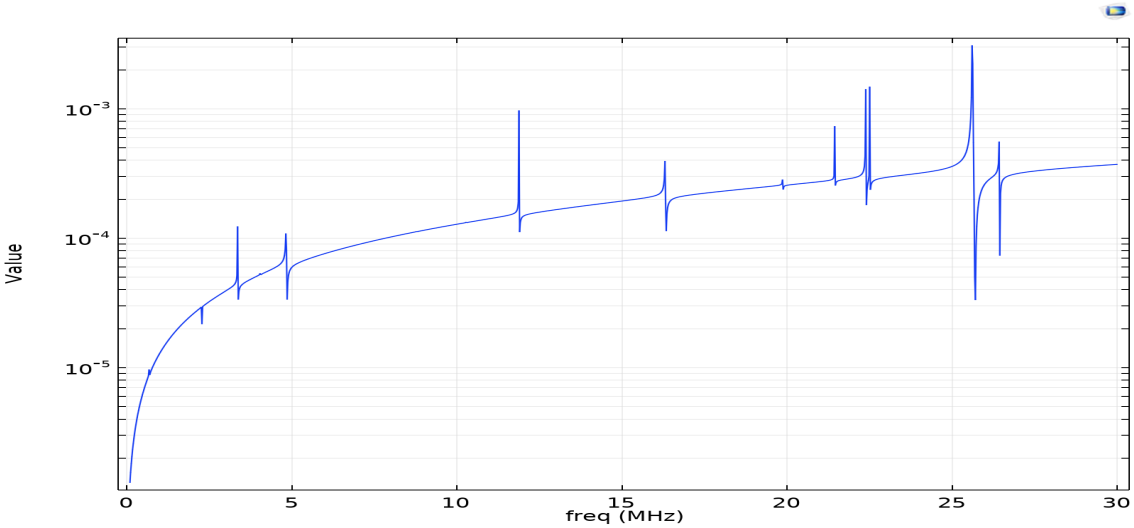

(b) 210 µm beam width, L-anchor

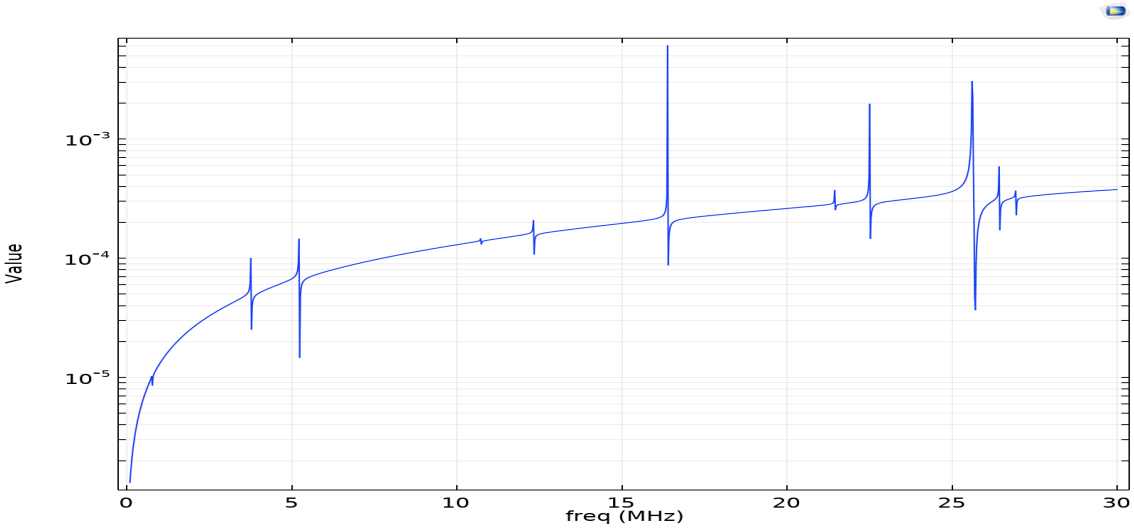

(c) 210 µm beam width, T-anchor

Figure 22: Spurious modes peaks analysis for 24-MHz resonators for 210 µm beam width with different anchor design

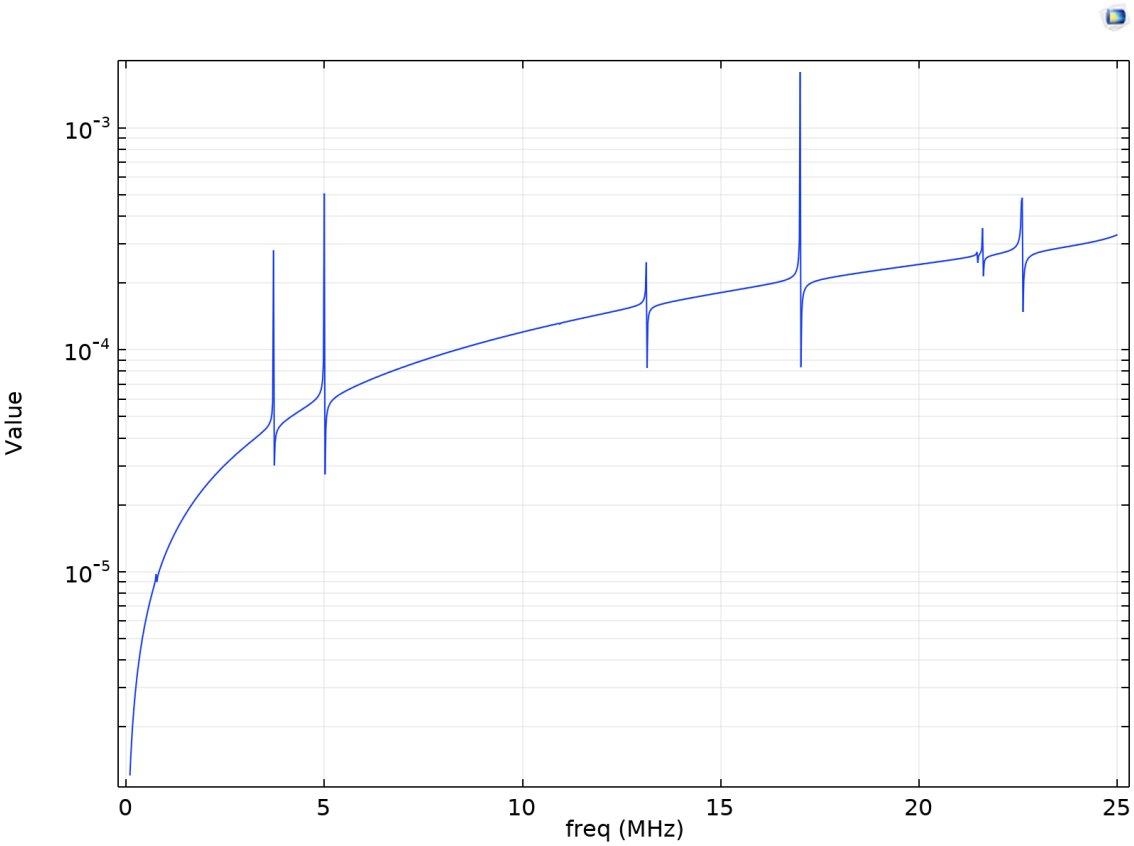

(a) 200 µm beam width, T-anchor

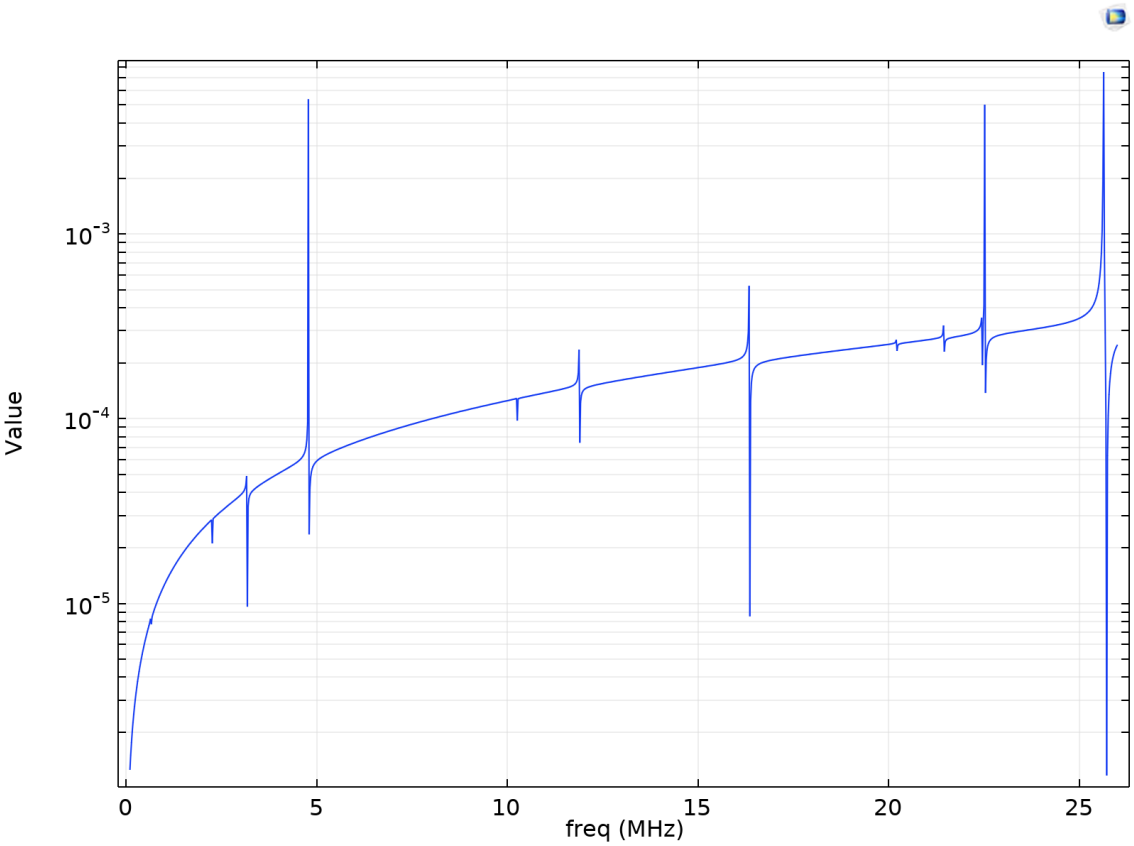

(b) 210 µm beam width, L-anchor

Figure 23: Spurious modes peaks analysis for 24-MHz resonators with different anchor tyoes and different beam widths

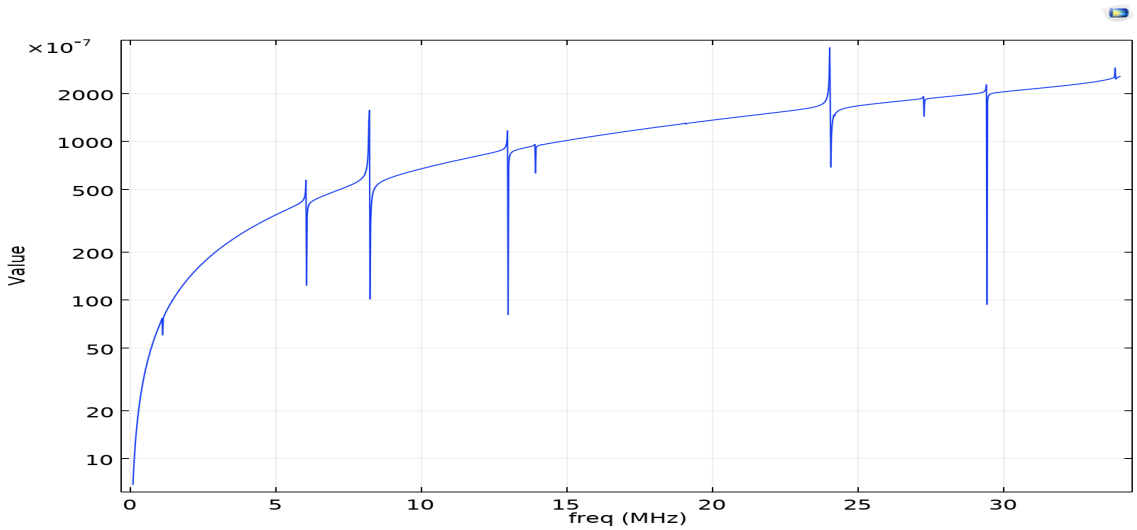

(a) 140 µm beam width, folded anchor

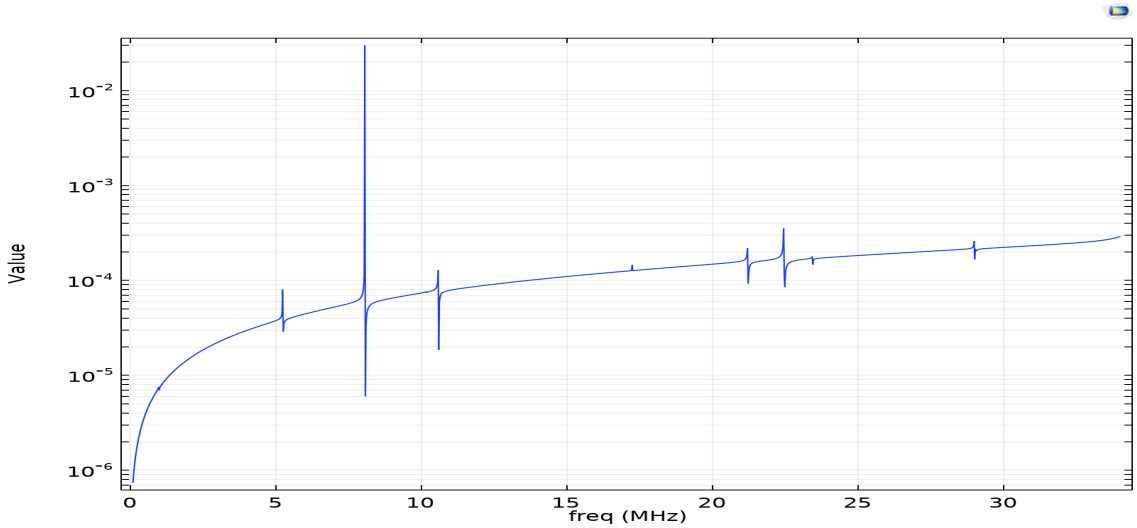

(b) 150 µm beam width, folded anchor

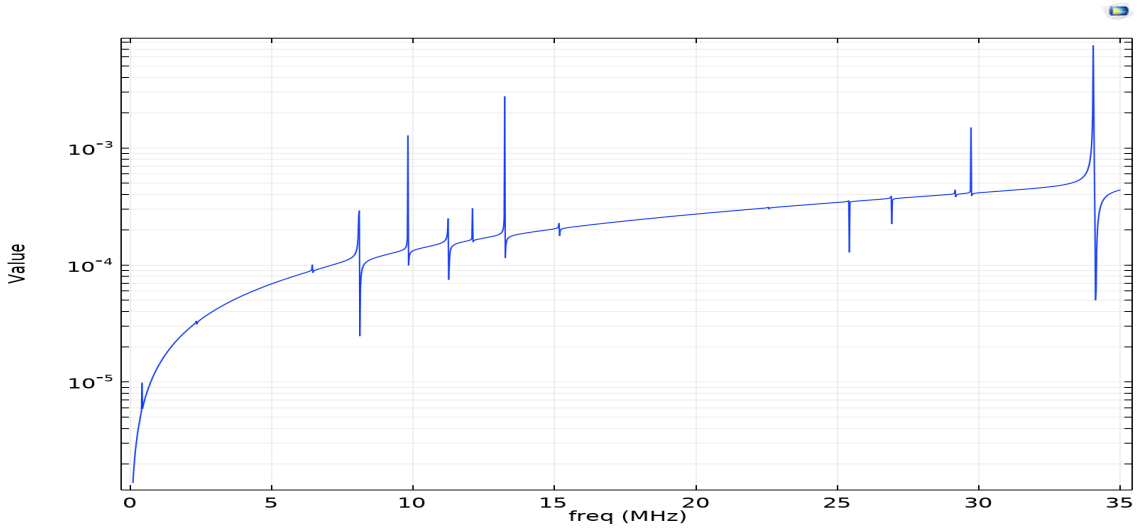

(c) 290 µm beam width, folded anchor

Figure 24: Spurious modes peaks analysis for 32-MHz F-anchor resonators with different beam widths

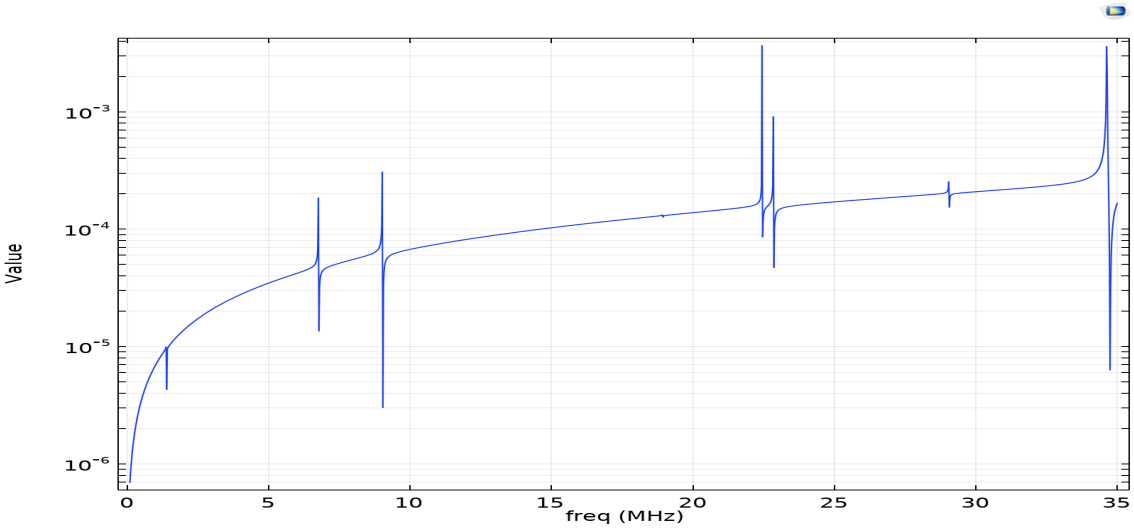

(a) 150 µm beam width, T-anchor

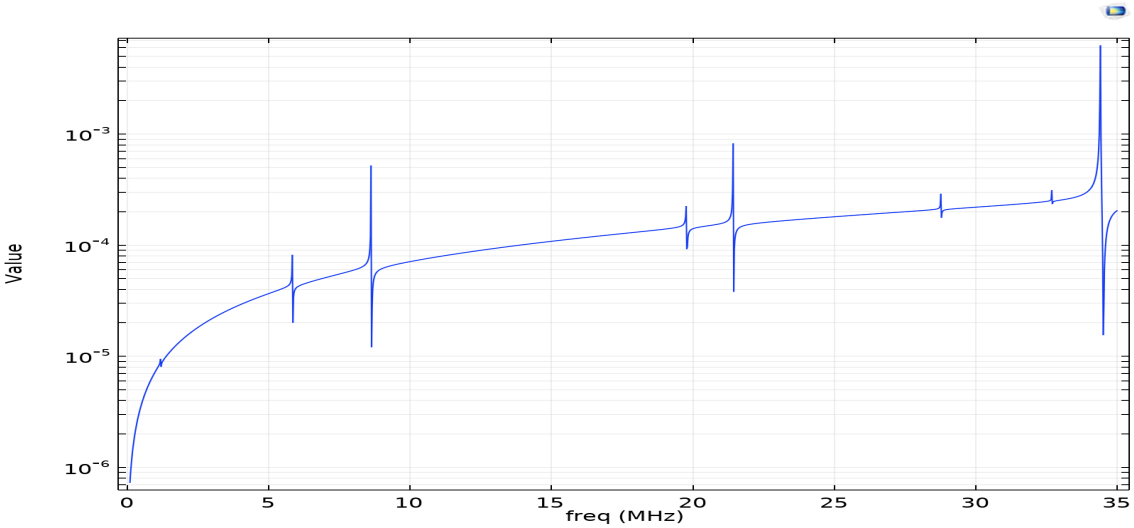

(b) 160 µm beam width, T-anchor

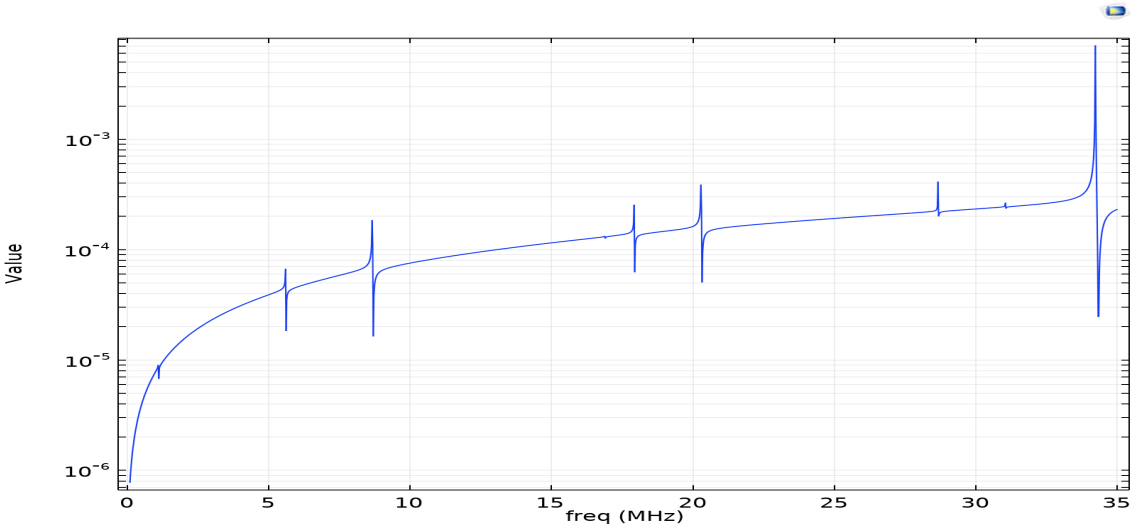

(c) 170 µm beam width, T-anchor

Figure 25: Spurious modes peaks analysis for 32-MHz T-anchor resonators for different beam widths

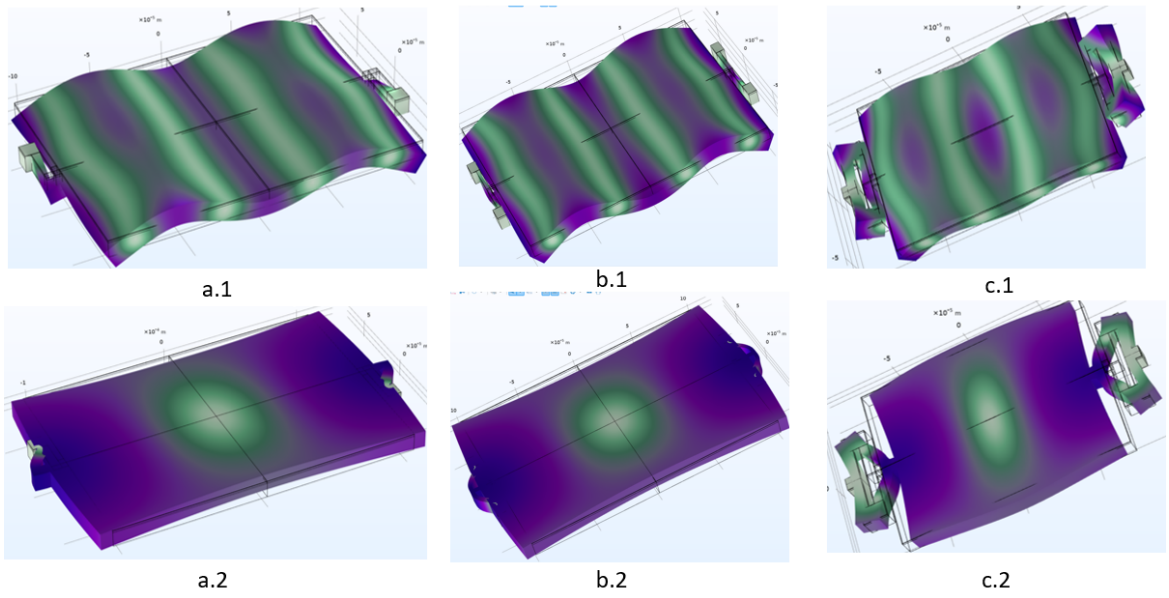

Figure 26: FEM simulations for spurious modes which are suspected to perform defects to the MEMS resonator, (a.1) and (a.2) show 2 spurious modes for L-shape anchor, (b.1) and (b.2) show 2 spurious modes for T-shape anchor and (c.1) and (c.2) show 2 spurious modes for folded spring shape anchor

4.2 Microfabrication processes

As a result of the microfabrication processes, there was a finding in the processed devices, as shown in figure 27, there were residuals of AlN nano particles in the trenches of the devices, those residuals were detected using scanning electron microscope (SEM). Figure 28 shows the measurements of the corresponding electrical response of the dies with the AlN residuals.

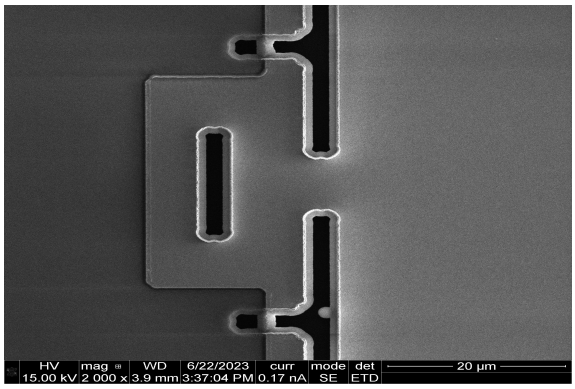

(a) T-anchor with AlN residuals

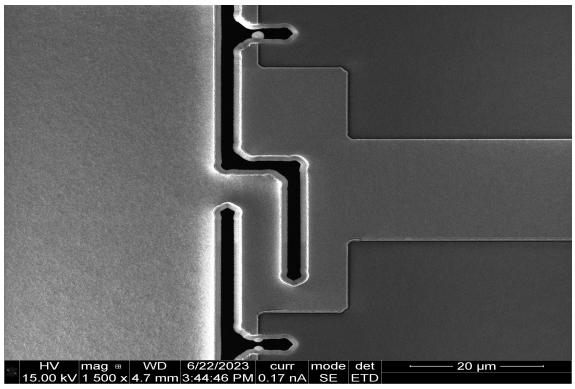

(b) L-anchor with AlN residuals

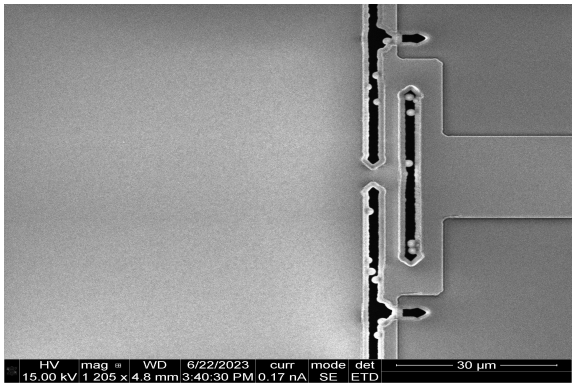

(c) T-anchor with AlN residuals

Figure 27: SEM images of AlN residuals in the trenches of the MEMS resonators anchors after microfabrication processes, few particles found in (a) and (b) while (c) contains more particles found in the trenches

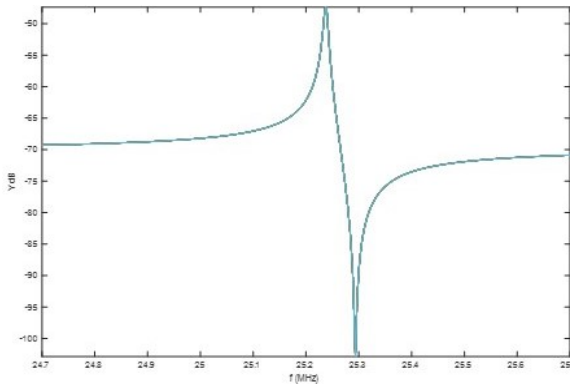

(a) Resonance frequency of the device shown in figure 27a

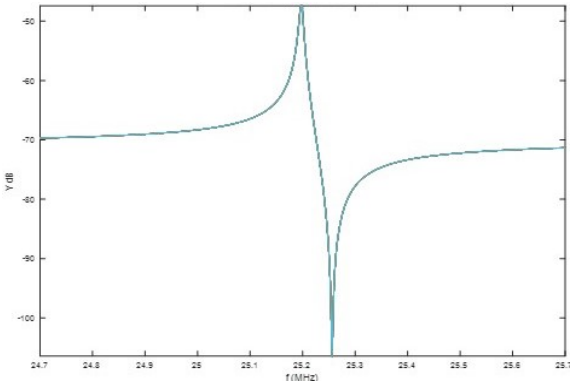

(b) Resonance frequency of the device shown in figure 27b

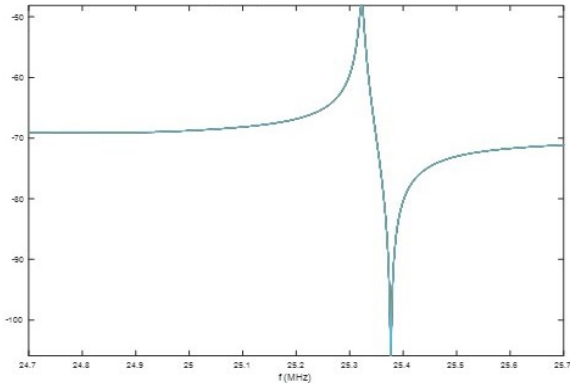

(c) Resonance frequency of the device shown in figure 27c

Figure 28: Measuring the resonance frequency of the dies with AlN nano-residuals

4.3 Electrical defects inducing

Figure 29 shows the percentage of the defected dies when stimulated in a frequency of a specific spurious mode as discussed in section 3.1.3. The experiment included 23MHz and 24MHz devices with different anchor types of T-shape anchor, L-shape anchor and Folded spring anchor which are mentioned in the figure.

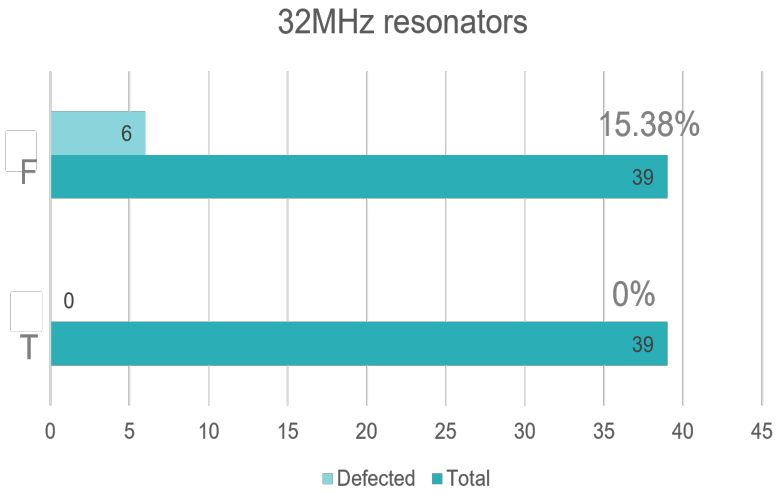

(a) Number of defected 32MHz dies to the total number of dies subjected to electrical stimulation

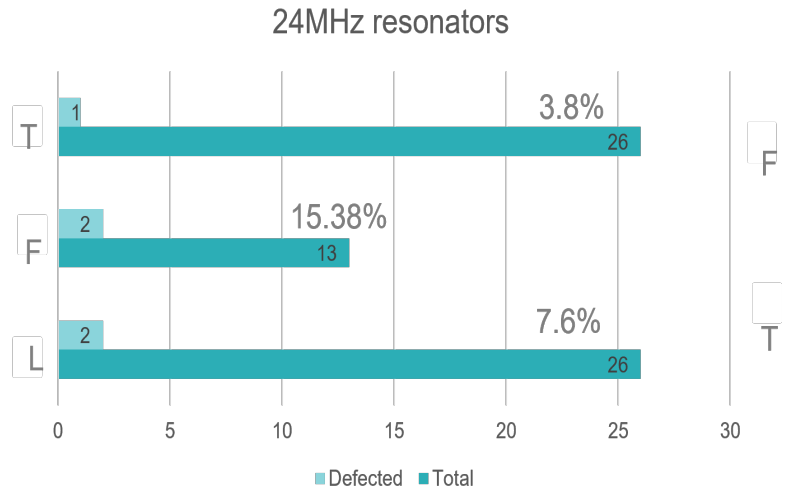

(b) Number of defected 24MHz dies to the total number of dies subjected to electrical stimulation

Figure 29: Result of defected dies for 24MHz and 32MHz resonator after electrical stimulation at spurious modes presented in figure 26

4.4 Tape peeling test

Tape peeling test resulted in micro cracks mainly present in the anchor as shown in figure 30, the percentages of the cracked anchors after the test are mentioned in figure 31, the anchors have different designs and dimensions.
Figure 32 shows the number of defected dies to the total number of dies, those dies were selected to have different anchor shape but share the same anchor dimensions, design 1, 2 and 3 from table 1.

Figure 30: A crack found in folded anchor after tape peeling test

4.5 Automatic optical inspection

The result of the AOI system for detection of defected dies after the tape peeling test is shown in figure 33, the result is visualized to represent the dies location in the wafer by the corresponding row and column numbers.
AOI system result was validated by using population of 400 dies which were checked manually for defects, and compared to the AOI results, AOI system showed a detection rate of 85.5% and a false positive of 7.1%.

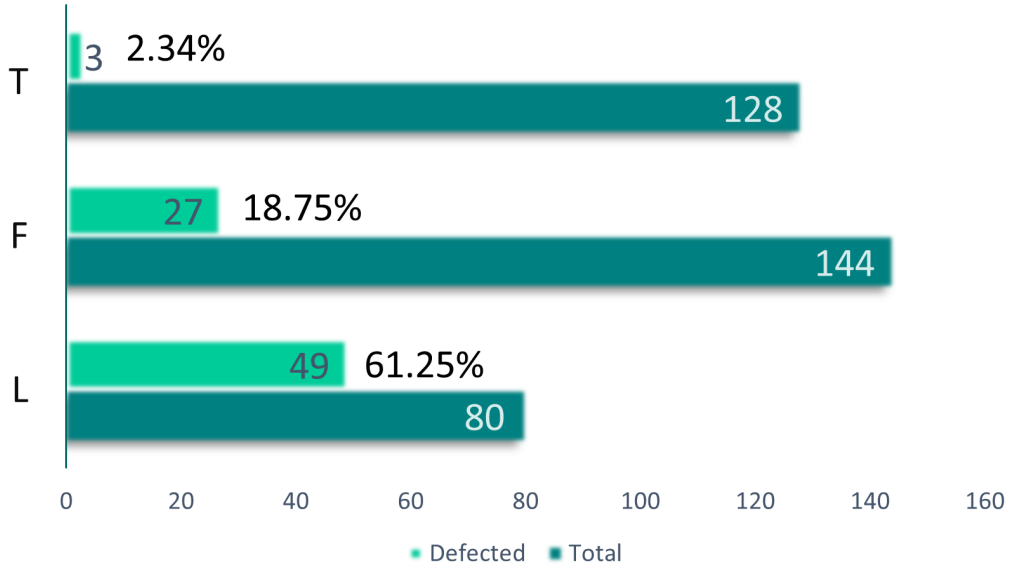

Figure 31: Percentage of cracked anchors to the total number of dies after tape peeling, for different dimensions anchor types

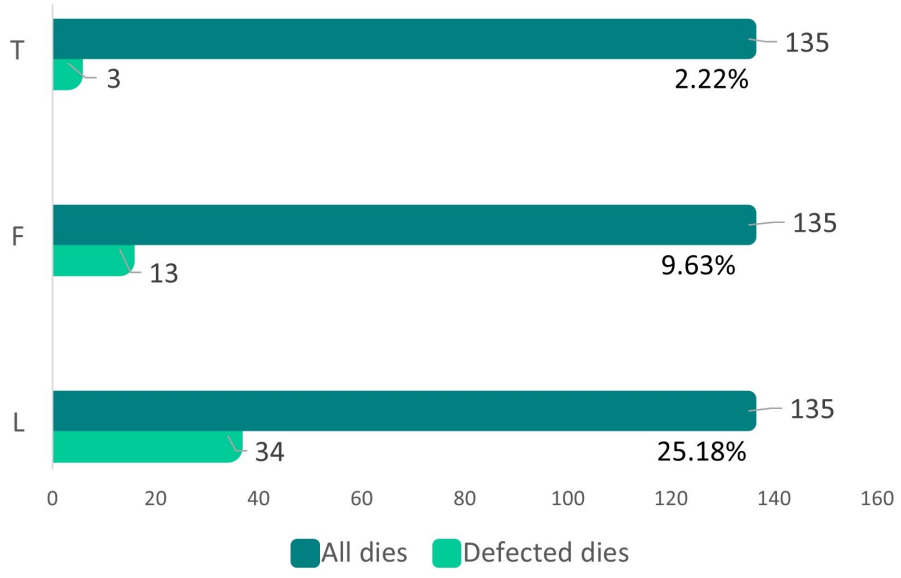

Figure 32: Percentage of cracked anchors to the total number of dies after tape peeling, for different anchor types with the same dimensions of 17µm spring length and 6µm spring width

Percentage of induced cracks	Anchor type	Test method	Resonator design
Lowest	T-anchor	Electrical inducing	32MHz
Highest	L-anchor	Tape peeling	24MHz

Table 3: The highest and lowest percentage of cracked anchors with the corresponding inducing method and design specifications

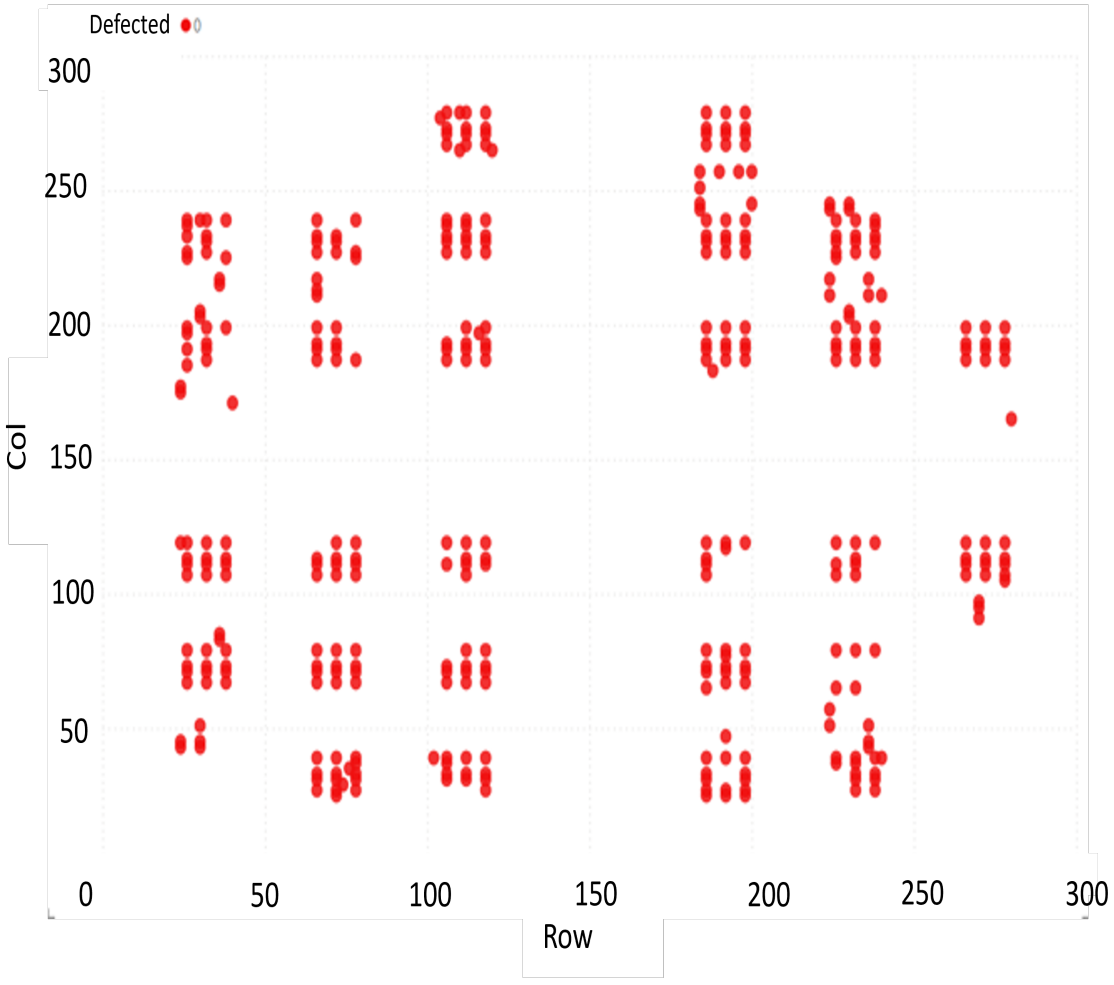

Figure 33: AOI detection and localization for the defected dies after the tape peeling, each die is represented in the corresponding row and column in the wafer

5 Discussion

5.1 MEMS resonator design

As this study is based on industrial research for Kyocera-tikitin oy KTO, the designed devices of 32MHz and 24MHz were chosen to align with KTO research needs. Figure 11 indicates that better quality factor values for 24-MHz resonator are populated in higher beam width values, therefor, the implemented designs have the values around 200 and 210 µm. On the contrary, figure 12 shows the 32-MHz resonator can have high quality factor values at lower beam width which resulted in using lower values for the resonator beam widths. For the aim to study the effect of using different spring dimensions in the quality factor values, figure 13 illustrates that the quality factor has lower dependency on the anchor spring dimensions as the graph shows close values for various combinations of spring lengths and widths, that resulted in dedicating the 32-MHz designs on studying the effect of the low and high anchor spring dimensions on the robustness of the anchor.
As illustrated in figure 14 L-anchor resonator shows low quality factor in the 32MHz design, hence, it is excluded from the implementation in the test wafer. For the implemented 24-MHz designs, the effect of the anchor design studied by the method of applying the same spring dimensions and resonator beam width for different anchor shapes, that is shown in table 1 where for designs 1,2 and 3 have a beam width of 210 µm and spring length and width of 17 and 6 µm respectively.
AlN thickness showed minor change of the quality factor as showed in figure 15, thus, the design were processed with 1.465 µm for process consideration of KTO wafers history.
Tables 1 and 2 include all the designs chosen to be implemented in this study, that is followed by the spurious mode analysis for the chosen designs. Figures from 22 to 25 represent the spurious modes analysis for the different implemented designs.
The geometry of the anchor has limited effect on the number of spurious modes which appears in figure 22 where the beam width is constant while the anchor type is different, the spurious analysis found to have the same number of modes.
The higher the beam width is, the more spurious modes which the device can resonate on, which can be noticed in the difference of number of peaks between figure 24a and figure 24c with 9 and 14 peaks for 140 and 290 µm beam width respectively, therefor, to exclude the unwanted spurious shapes, designing lower beam width devices can be adopted as a part of the solution.
Figure 26 shows the spurious modes selected to induce the electrical defects, the figure shows the deformation happens in the anchor for two modes, the selected mode shapes were found in all designs with variant frequencies depending on the design with 3 MHz range.
The effect of the dual-shell gyroscope geometry was discussed by Wei G. [62], the quality factor dependency on the anchor geometry of the anchor in the study was more distinct. The study proposed a ratio between dimensions to be the identifier, which is different approach than what presented in this study where sweeping values of anchor dimensions were implemented. A ration between the spring length and

spring width can be adopted approach as future work for the aim of minimizing the anchor dimensions with maintaining the same robustness of device.

5.2 Microfabrication defects

Figure 28 indicates that the residuals found in the trenches have almost no electrical affect on the resonance frequency of the devices, since AlN is an electrical insulator, this result was expected as there is no electrical conductivity needed in the trench area. On the other hand, an electrical damage could occur if the particles were formed of a conductive material, as a result of that, the electrical property of the device would be severely affected.
As a result of another etching process, silicon residuals can be found on trenches as a result of different etching rates which can cause an electrical properties damage for the device [46]. The result of the microfabrication defects is process dependent, the residuals shown in this study were a result of the AlN etching process, while in other microfabrication processes other defects can be found with different levels of severity.

5.3 Defects inducing and detection

the defects captured during the operational mode which was referred to as electrical induced defects, in addition to the defects formed due to tape peeling method were mainly microcracks in the anchor which has the weakest beams due to the small dimensions, the cracks mainly had the length of 4-8 µm, a sample of the induced cracks can be found in figure 30. Other designs beside the solid beam resonator presented in this work, might be subjected to different localization of cracks as well as different dimensions.
From the results presented, the defects induced electrically are less probable to be formed specially if low power was used for the electrical stimulation. That is affected by the probability of the device resonating in the specified frequency, considering the study was obtained using the highest deformation got form the spurious shapes. The electrical defects made an initial result of the robustness of the T-shape anchor over the F and L shape anchors. The selection made for the dies used in the electrical inducing was made with aim of including all designs implemented in tables 1 and 2. Since 32MHz showed very low quality factor for the L-anchor, no such anchor was implemented in the 32MHz design, which led to uncertainty about the robustness of the F-anchor and L-anchor geometries.
To support the agility of some anchor shapes compared to others, tape peeling test was done across the whole silicon wafer, the result in figure 31 supported the result of the electrical defects inducing mentioned above, in which the T-anchor had the least percentage of defected dies compared to the L-anchor and F-anchor with a remarkably higher percentage of defected L-anchor which exceeded 60%.
In order to get the opportunity to study the affect of the anchor geometry solely, design 1, 2 and 3 from table 1 were selected for the purpose of studying the geometry over the dimensions, in which same dimensions of 17µm spring length with 6µm spring width were implemented with different anchor geometry, the result obtained

in figure 32 continued to the same order of strength pattern, which excluded the dimensions affect, quarter of the L-anchor dies were cracked while only 9.63% and 2.22% of F-anchor and T-anchor respectively were cracked.
The cracked devices from the tape peeling method were used to validate the AOI result, by manually checking the cracked dies and compared them to the detection of the AOI system. The result of AOI was mainly affected with the auto-focus module that is built-in the AOI setup, the blurry pictures affected the detection rate of the dies by the system, moreover, it resulted in false positives results. The detection rate of 85.5% needs better enhancement and deeper focus than the 7.1% false-positive result, that's because of the high severity of not detecting cracks than falsely indicating ones.
Although tape peeling test is mainly carried out to ensure the adhesion of the deposited layers [63][64]. Tape peeling can be used to study the probability of defects formation on devices, Michael H. study found out 6.7% of MEMS dies were defected after tape peeling test [65], the differences between results are due to MEMS structure differences, the tape adhesion and the mechanical removing of the tape.
The technique of combining optical inspection and electrical testing arose with the experimental proof that 80% of the defects found optically were not detected with the electrical testing [66]. That highlighted the importance of detecting defects that have less electrical impact on the characteristics of the device, although they have optically detected defects on the structure of the device.

6 Conclusion

With the escalating demand of the time reference devices, MEMS resonator is rising as a good candidate to take this function over other devices such as quartz resonator. Because of the research and development focusing on MEMS resonators, it is expected that MEMS resonator will achieve excellent efficiency with high quality factor and small size which is a needed feature to reduce cost and facilitate the integration with other electronics.
Studying the reasons of the defects formation in MEMS devices would help significantly to avoid such problems in design and manufacturing. For unavoidable defects with the aim of developing better MEMS devices, better defects inspections tools is needed specially with the mass production. The micrometer size of MEMS resonator with the microcracks appearing throughout the manufacturing or operation initiate the need for high quality inspection mechanisms.
This study starts with the design of different MEMS devices in which different parameters were taken under consideration, the quality factor optimization process showed less dependency on the anchor type and dimensions compared to the resonator beam dimensions, moreover, the dependency in the AlN thickness variance in small scale was almost negligible. The design phase with the spurious mode analysis indicated the probability of the defects formation because of the spurious mode, while the microfabrication defects were considered because of the experience with such processes.
The results concluded that the number of defects that can be induced during the operation of the device is lower than the expected number, although, for this operational experiment, the spurious modes used were severely deforming a sensitive part such as the anchor. The percentage of dies which were defected electrically didn't exceed 9%. The main dependency of the strength of the device was due to the geometry of the anchor and less dependency on the dimension of the anchor. The hypothesis of the strength of specific anchor shapes over others was supported with the tape peeling test which showed obvious strength dependency on the anchor geometry.
Defects inspection importance shaped the last part of the study, where an optical inspection system was proven to reduce the time needed for full wafer inspection. The enhancement for the system can be done for faster and nanocracks detection by enhancing the magnifier lens used, and better alignment for the auto-focus module. An electrical inspection can be done as well, although it is recommended to start with AOI first as it is fast, more reliable and needs less statistical analysis from the user. AOI resulted in 15% undetected defects which can be transferred and detected by the second stage of the electrical inspection where more statistical analysis might be needed. Electrical detection can be implemented by scanning wider range of frequencies, analyse the spurious modes which can be used for the detection by implementing statistical methods to differentiate between the defected and non-defected devices with a similar methodology as in 2.7.2.
Further study can be conducted by testing the effect of deeper hidden cracks, the effect on the quality factor and the resonance characteristics of the device. The test

can be carried out by using IR imaging as non-destructive test, or destructively by removing the outer layer of the electrode and check the piezoelectric and silicon layers as basic step for validation purposes.

References

[1] L. Comenencia Ortiz et al., *"Low-Power Dual Mode MEMS Resonators With PPB Stability Over Temperature," J. Microelectromech. Syst.,* 2020. https://doi.org/10.1109/jmems.2020.2970609

[2] Verma, G., Mondal, K., Gupta, A. *"Si-based MEMS resonant sensor: A review from microfabrication perspective," Microelectronics Journal,* 2021. https://doi.org/10.1016/j.mejo.2021.105210

[3] M. Bau', M. Zini, A. Nastro, M. Ferrari, V. Ferrari, and J. E. Y. Lee, *"Electronic technique and system for non-contact reading of temperature sensors based on piezoelectric MEMS resonators," in 2022 IEEE Int. Symp. Circuits Syst. (ISCAS),* 2022. https://doi.org/10.1109/iscas48785.2022.9937328

[4] M. Bharati, L. Rana, R. Gupta, A. Sharma, P. K. Jha, and M. Tomar, *"Realization of a DNA biosensor using inverted Lamb wave MEMS resonator based on ZnO/SiO2/Si/ZnO membrane," Analytica Chimica Acta,* 2023. https://doi.org/10.1016/j.aca.2023.340929

[5] L. Wang et al.,*"A Review on Coupled Bulk Acoustic Wave MEMS Resonators," Sensors,*2022.https://doi.org/10.3390/s22103857

[6] Jaakkola, A. *"Piezoelectrically transduced temperature compensated silicon resonators for timing and frequency reference applications," PhD Dissertation, Department of Applied Physics, Aalto university, Finland,* 2016.

[7] K. R. Cioffi and Wan-Thai Hsu, *"32KHz MEMS-based oscillator for low-power applications," in 2005 IEEE Int. Freq. Control Symp. Exposition,*2005.https://doi.org/10.1109/freq.2005.1573992

[8] *"MEMS for Cell Phones and Tablets." PR Newswire: press release distribution, targeting, monitoring and marketing.* Accessed Jat: Jul. 29, 2023). Available at: https://www.prnewswire.com/news-releases/mems-for-cell-phones-and-tablets-219795091.html

[9] J. Li, T. Mattila, and V. Vuorinen, *"MEMS Reliability," in Handbook of Silicon Based MEMS Materials and Technologies. Elsevier,* 2015, https://doi.org/10.1016/b978-0-323-29965-7.00041-5

[10] C.-L. Wong and W.-K. Wong, *"In-plane motion characterization of MEMS resonators using stroboscopic scanning electron microscopy," Sensors Actuators A: Physical, vol. 138, no. 1, p. 167–178,* 2007.https://doi.org/10.1016/j.sna.2007.04.046

[11] I. Chasiotis and W. G. Knauss, *"A new microtensile tester for the study of MEMS materials with the aid of atomic force microscopy," Exp. Mechanics,*. 2002. https://doi.org/10.1007/bf02411051

[12] R. Asgary, K. Mohammadi, and M. Zwolinski, *"Using neural networks as a fault detection mechanism in MEMS devices,"* *Microelectronics Rel.,* 2007. https://doi.org/10.1016/j.microrel.2006.04.012

[13] F. Solazzi, *"Novel Design Solutions for High Reliability RF MEMS Switches,"* doctoral thesis, Università degli studi di Trento, 2011. Accessed: Jul. 29, 2023. [Online]. Available: https://hdl.handle.net/11572/369154

[14] *World's smallest MEMS gyroscope for navigation.*, Flaherty. Accessed: 08 June 2023. eeNews Europe. Available at: https://www.eenewseurope.com/en/worlds-smallest-mems-gyroscope-for-navigation/#:~:text=French%20research%20lab%20CEA%2DLeti,millimeters%20using%20nano%2Dresistive%20sensing.

[15] *Murata Sca3300 High Performance 3 Axis MEMS accelerometer targets industrial and Automotive Applications.*, Murata Manufacturing Co., Ltd. Accessed: 08 June 2023. Available at: https://www.murata.com/en-eu/news/sensor/accel/2016/1102

[16] L. Wei et al., *"The Recent Progress of MEMS/NEMS Resonators,"* *Micromachines, vol. 12, no. 6, pp. 724,* 2021. https://doi.org/10.3390/mi12060724

[17] N. Deb, S. V. Iyer, T. Mukherjee, and R. D. S. Blanton, *"MEMS resonator synthesis for testability,"* *in Design, Test, Microfabr. MEMS/MOEMS, B. Courtois, S. B. Crary, W. Ehrfeld, H. Fujita, J. M. Karam, and K. W. Markus, Eds. Paris, France. SPIE, 1999,* 2023. https://doi.org/10.1117/12.341153

[18] Walker, J., Halliday, D., Resnick, R. *"Fundamentals of Physics: Extended, With Modern Physics (Fundamentals of Physics),"* *John Wiley & Sons Inc.,* 2005.

[19] Drieberg, M., Sahoo, N. C. *"On resonance and frequency response characteristics of electrical circuits,"* *The International Journal of Electrical Engineering*, 2013. https://doi-org.libproxy.aalto.fi/10.7227/IJEEE.50.4.3

[20] Storr, W. (2022, August 8). Series resonance in a series RLC resonant circuit. *B*asic Electronics Tutorials. Retrieved May 2, 2023, from https://www.electronics-tutorials.ws/accircuits/series-resonance.html

[21] Wang, Z., Li, M., & Wang, R. *"Resonance beyond frequency-matching: multi-dimensional resonance,"* *New Journal of Physics,* 2017. https://doi.org/10.1088/1367-2630/aa6275

[22] Lu, Y., Tang, H.-Y., Fung, S., Boser, B. E., Horsley, D. A.*"Pulse-Echo Ultrasound Imaging Using an AlN Piezoelectric Micromachined Ultrasonic Transducer Array With Transmit Beam-Forming,"* *Journal of Microelectromechanical Systems,* 2016. https://doi.org/10.1109/JMEMS.2015.2503336

[23] Partridge, A., Lee, H.-C., Hagelin, P., Menon, V. *"We know that MEMS is replacing quartz. But why? And why now?," Joint European Frequency and Time Forum & International Frequency Control Symposium (EFTF/IFC),* 2013. https://doi.org/10.1109/EFTF-IFC.2013.6702311

[24] Hopcroft, M. A., Agarwal, M., Park, K. K., Kim, B., Jha, C. M., Candler, R. N., Yama, G., Murmann, B., Kenny, T. W. *"Temperature Compensation of a MEMS Resonator Using Quality Factor as a Thermometer," 19th IEEE International Conference on Micro Electro Mechanical Systems,* 2006. https://doi.org/10.1109/MEMSYS.2006.1627776

[25] Ahmed, S., Li, R., Zou, X., Al Hafiz, M. A., Fariborzi, H. *"Modeling and Simulation of A MEMS Resonator Based Reprogrammable Logic Gate Using Partial Electrodes," In 2019 Symposium on Design, Test, Integration & Packaging of MEMS and MOEMS (DTIP). IEEE,* 2019. https://doi.org/10.1109/DTIP.2019.8752880

[26] Hsu, W.-t. *"Vibrating RF MEMS for Timing and Frequency References," 2006 IEEE MTT-S International Microwave Symposium Digest,*, 2006. https://doi.org/10.1109/MWSYM.2006.249704

[27] Wu, G., Xu, J., Ng, E. J., Chen, W. *"MEMS Resonators for Frequency Reference and Timing Applications," Journal of Microelectromechanical Systems*, 2020. https://doi.org/10.1109/JMEMS.2020.3020787

[28] Zou, X., Ahmed, S., Jaber, N., Fariborzi, H. *"A Compact High-Sensitivity Temperature Sensor using an Encapsulated Clamped-Clamped Mems Beam Resonator," International Conference on Solid-State Sensors, Actuators and Microsystems (Transducers). IEEE,* 2021. https://doi.org/10.1109/Transducers50396.2021.9495651

[29] Zhao, C., Montaseri, M. H., Wood, G. S., Pu, S. H., Seshia, A. A., Kraft, M. *"A review on coupled MEMS resonators for sensing applications utilizing mode localization," Sensors and Actuators,* 2016. https://doi.org/10.1016/j.sna.2016.07.015

[30] Viard, R., Talbi, A., Ghouila-Houri, C., Kourta, A., Merlen, A., Pernod, P. *"Magneto-mechanical micro-valve for active flow control," Sensors and Actuators,* 2020. https://doi.org/10.1016/j.sna.2020.112387

[31] Sathya, S., Pavithra, M., Muruganand, S. *"Simulation of Electrostatic Actuation in Interdigitated Comb Drive MEMS Resonator for Energy Harvester Applications," IOP Conference Series: Materials Science and Engineering,* 2016. https://doi.org/10.1088/1757-899X/149/1/012050

[32] Rana, M., Pande, R., Kukreti, K. *"Design of RF MEMS Piezoelectric Disk Resonator for 5G Communication," Materials Today: Proceedings,* 2022. https://doi.org/10.1016/j.matpr.2022.08.503

[33] Chen, Z., Kan, X., Yuan, Q., Wang, T., Yang, J., Yang, F. *"A Switchable High-Performance RF-MEMS Resonator with Flexible Frequency Generations,"* *Scientific Reports,* 2020. https://doi.org/10.1038/s41598-020-61744-2

[34] W.N. Sharpe. *"Mechanical properties of MEMS materials, Introduction and Fundamentals,"* 2005.

[35] R. Pratap, A. Arunkumar, *Material selection for MEMS devices.*, 2007.

[36] *A MEMS Clearinghouse and information portal for the MEMS and Nanotechnology community.*, Fabricating MEMS and nanotechnology. Accessed: May 5, 2023. Available at: https://www.memsnet.org/about/fabrication.html

[37] Abdolvand, R., Bahreyni, B., Lee, J., Nabki, F. *"Micromachined Resonators: A Review. Micromachines"*, 2016.

[38] Kluba, M. M., Li, J., Parkkinen, K., Louwerse, M., Snijder, J., Dekker, R. *"Cavity-BOX SOI: Advanced Silicon Substrate with Pre-Patterned BOX for Monolithic MEMS Fabrication,"* *Micromachines.*, 2021. https://doi.org/10.3390/mi12040414

[39] Shi, L.; Piazza, G.*"Lithium Niobate on Silicon Dioxide Suspended Membranes: A Technology Platform for Engineering the Temperature Coefficient of Frequency of High Electromechanical Coupling Resonators,"* *Journal of Microelectromechanical Systems* , 2014. https://doi.org/10.1109/JMEMS.2014.2312888

[40] Demirci, M.U., Nguyen, C.T.C. *"Mechanically Corner-Coupled Square Microresonator Array for Reduced Series Motional Resistance,"* *Journal of Microelectromechanical Systems,* 2006. https://doi.org/10.1109/JMEMS.2006.883588

[41] Li, S.-S., Lin, Y.-W., Ren, Z., Nguyen, C.T.-C. *"An MSI Micromechanical Differential Disk-Array Filter,"* *TRANSDUCERS 2007 - 2007 International Solid-State Sensors, Actuators and Microsystems Conference,* 2007. https://doi.org/10.1109/SENSOR.2007.4300130

[42] Zhao, C., Montaseri, M. H., Wood, G. S., Pu, S. H., Seshia, A. A., Kraft, M. *"A review on coupled MEMS resonators for sensing applications utilizing mode localizatio,"* *Sensors and Actuators A: Physical,* 2016. https://doi.org/10.1016/j.sna.2016.07.015

[43] Pattanaik, P.,Ojha, M. *"Review on challenges in MEMS technology,"* *Materials Today: Proceedings,* 2021. https://doi.org/10.1016/j.matpr.2021.03.142

[44] D. Joachim, L. Lin *"Characterization of selective polysilicon deposition for MEMS resonator tuning,"* *Journal of Microelectromechanical Systems,* 2003. https://doi.org/10.1109/JMEMS.2003.809967

[45] *Current challenges.* Accessed: 08 June 2023. MEMS and nanotechnology exchange. Available at: https://www.mems-exchange.org/MEMS/challenges.html

[46] Xie, J. *"Fabrication challenges and test structures for high-aspect-ratio SOI MEMS devices with refilled electrical isolation trenches" Microsyst Technol 21,*, 2014. https://doi-org.libproxy.aalto.fi/10.1007/s00542-014-2357-7

[47] Ge, C., Cretu, E. *"Simple and Robust Microfabrication of Polymeric Piezoelectric Resonating MEMS Mass Sensors," Sensors 2022,* , 2022. https://doi.org/10.3390/s22082994

[48] Deshpande, P. P., Pande, R. S., Patrikar, R. M. *"Fabrication and characterization of zinc oxide piezoelectric MEMS resonator," Microsystem Technologies,*, 2020. https://doi.org/10.1007/s00542-019-04509-w

[49] Kant Bajpai, V., Kumar Mishra, D., Dixit, P. *"Fabrication of Through-glass Vias (TGV) based 3D microstructures in glass substrate by a lithography-free process for MEMS applications," Applied Surface Science,* 2022. https://doi.org/10.1016/j.apsusc.2022.152494

[50] Kemppainen, J., Mattila, T., Paulasto-Krockel, M. *"Adhesion evaluation of the heat resistant pressure sensitive adhesives at elevated temperatures for MEMS gyroscope testing," 2011 International Symposium on Advanced Packaging Materials (APM),* 2011. https://doi.org/10.1109/ISAPM.2011.6105733

[51] Schroeder, W., Wolff, I. *The origin of spurious modes in numerical solutions of electromagnetic field eigenvalue problems," IEEE Transactions on Microwave Theory and Techniques,* 1994. https://doi.org/10.1109/22.285071

[52] Puder, J. M., Pulskamp, J. S., Rudy, R. Q., Polcawich, R. G., Bhave, S. A. *"A Method for the Suppression of Multiple Spurious Modes," Journal of Microelectromechanical Systems,* 2018. https://doi.org/10.1109/JMEMS.2018.2793100

[53] Young, H. T., Chiou, H. S., Huang, W. R. *"AOI strategies for defects identification of micro-electro mechanical system elements," Advances in Materials and Processing Technologies,* 2016. https://doi.org/10.1080/2374068X.2016.1147790

[54] Yang Yuan-Fu. *"A deep learning model for identification of defect patterns in semiconductor wafer map," 2019 30th Annual SEMI Advanced Semiconductor Manufacturing Conference (ASMC),* 2019. https://doi.org/10.1109/ASMC.2019.8791815

[55] Ralf B. *"Defect inspection strategies for 14 nm semiconductor technology," Proceedings of SPIE - The International Society for Optical Engineering,* 2012. https://doi.org/10.1117/12.928664

[56] Si-ChenPan, Kuo-Shen Chen. *"Design and Control of an Active Stage for Suppressing Motion Induced Vibration in Optical Inspection Systems," 2022 20th International Conference on Mechatronics - Mechatronika (ME),* 2019. https://doi.org/10.1109/ME54704.2022.9982985

[57] Chen, P.-C., Lin, Y.-T., Truong, C.-M., Chen, P.-S., Chiang, H.-K. *"Development of an Automated Optical Inspection System for Rapidly and Precisely Measuring Dimensions of Embedded Microchannel Structures in Transparent Bonded Chips,"* *Sensors 2021,* 2021. https://doi.org/10.3390/s21030698

[58] Shoaib, M., Hamid, N. H., Malik, A. F., Zain Ali, N. B., Tariq Jan, M. *"A Review on Key Issues and Challenges in Devices Level MEMS Testing,"* *Journal of Sensors,* 2016. https://doi.org/10.1155/2016/1639805

[59] Hantos, G., Flynn, D., Desmulliez, M. P. Y. *"Built-In Self-Test (BIST) Methods for MEMS: A Review,"* *Micromachines 2021,* 2020. https://doi.org/10.3390/mi12010040

[60] COMSOL Multiphysics® v. 6.1. www.comsol.com. COMSOL AB, Stockholm, Sweden.

[61] The MathWorks, Inc. (2022). Optimization Toolbox version: 9.4 (R2022b). Accessed: January 01, 2023. Available: https://www.mathworks.com

[62] W. Guan, D. Wang, M. H. Asadian, Y. Wang, and A. M. Shkel, *"Effect of Geometry on Energy Losses In Fused Silica Dual-Shell Gyroscopes,"* *in 2022 IEEE Int. Symp. Inertial Sensors Syst. (INERTIAL), Avignon, France,* 2022. https://doi.org/10.1109/inertial53425.2022.9787718

[63] L. Kang et al., *"A flexible resistive temperature detector (RTD) based on in-situ growth of patterned Ag film on polyimide without lithography,"* *Microelectron. Eng.,* 2023. https://doi.org/10.1016/j.mee.2019.111052

[64] V. Kant Bajpai, D. Kumar Mishra, and P. Dixit, *"Fabrication of Through-glass Vias (TGV) based 3D microstructures in glass substrate by a lithography-free process for MEMS applications,"* *Appl. Surf. Sci.,* 2023. https://doi.org/10.1016/j.apsusc.2022.152494

[65] M. Hall, *"Exploration of an adhesive peel test for failure and crack analysis of overmoulded MEMS packages,"* *Master thesis, Aalto univeristy,* 2020

[66] A. A. R. M. A. Ebayyeh and A. Mousavi, *"A Review and Analysis of Automatic Optical Inspection and Quality Monitoring Methods in Electronics Industry,"* *IEEE Access,* 2020. https://doi.org/10.1109/access.2020.3029127